Flow Localisation in a Crystal Bearing Magma

Laurence Wayne

Department of Earth Sciences, Durham University

2020/2021

This dissertation is submitted in partial fulfilment of the requirements for the degree BSc Geophysics with Geology

Online version

The code appendix and figures from other published works have been removed for copyright reasons. Each removed figure keeps its caption and citation, so it can be found in the original paper.

Abstract

The dynamics of magma ascent in volcanic conduits plays a large role in determining the style of eruption at the Earth's surface. Here, a physical model solving for the relative phase velocities of particles in dense granular suspensions is utilised to explore the phenomenon of crystal migration. The model is based on Lecampion & Garagash, 2014, using the rheological framework of Boyer, et al., 2011.

This dissertation seeks to make the first application of this physical model to a magmatic setting by applying case study examples of volcanoes to the dimensional result and assessing the output. The case study values used in the code are found from previous literature for each example. In this way, the extent to which crystal migration is occurring in the natural system as a function of differing magma type can be investigated. Case studies for each different magma type of Basaltic, Andesitic and Dacitic are used in the code. This includes the use of 'extreme' examples, chosen to give the best chance of seeing crystal migration under natural conditions. The results found from implementation of these case studies into the code is that there is no situation on Earth where crystal migration is possible.

The rheology of magmas has been found to be non-Newtonian following previous small-scale experiments, such as Caricchi, et al., 2007. That conclusion, obtained from those studies was due to crystal migration occurring in the samples, however the crystal migration theory was not available at the time of those experiments, and so was overlooked. As shown in this dissertation, crystal migration does not occur on these large-scale conduit sizes. This gives the conclusion that the rheological behaviour of magma on conduit-scale sizes is in fact Newtonian. Therefore, the results of these small-scale experiments are an experimental artefact and are not up-scalable to conduit sizes. Implications for this result are that previous

models of magma ascent may need to be revisited due to inappropriate use of non-Newtonian rheology during simulation.

Preamble

Much of the theory work used as a basis for this dissertation is taken from Lecampion & Garagash, 2014, titled 'Confined flow of suspensions modelled by a friction rheology'. The model defined in that study for flow of particles in a pipe is applied here to the case of crystal-bearing magma flow in a volcanic conduit. The theory for Lecampion & Garagash, 2014 is heavily reliant on Boyer, et al., 2011, so credit is also passed there.

The model from Lecampion & Garagash, 2014 was originally coded up verbatim by the external supervisor to this dissertation, Dr. Jérémie Vasseur in 2016. This code is utilised here to apply the model numerically to the case of magmatic systems, as described in later sections.

This work turns the theoretical models produced from the aforementioned studies into a real conclusion about natural magmatic systems. From the debt owed to those earlier studies, data produced from work in this dissertation enables conclusions on the rheology of magmas on conduit scale sizes to be drawn.

Contents

Abstract **2**

Preamble **3**

1 Introduction **5**

1.1 Background physics 7

1.2 Initial Applications to Magmatic Systems 8

1.3 Field Evidence 9

1.4 Objectives & Hypotheses 11

1.5 Relative Importance 11

2 Background and Methods 12

2.1 Introduction 12

2.2 Model Description 12

2.2.1 Cartesian vs Cylindrical 13

2.2.2 Applied Rheology and Viscous Number 13

2.2.3 Origin of Viscous Number from Inertial Number 14

2.2.4 Continuum Model 15

2.2.3 Numerical procedure 17

2.2.5 Steady State Flow to find Particle Pressure 18

2.2.6 Mean Pressure Gradient 19

2.2.7 Strain Rate, Particle Volume Fraction and Flow Velocity 20

2.3 Outputs 20

3. Dimensionless Results 21

3.1 Introduction 21

3.2 Scaling Parameters 21

3.3 Results 22

3.3.1 Particle Volume Fraction Concentration 23

3.3.2 Strain Rate vs Radial Position 23

3.3.3 Axial Velocity vs Radial Position 23

3.3.4 Magma Pressure Gradient vs Axial Position 24

3.3.5 Gap Averaged Crystal Volume Fraction vs Axial Position 25

3.4 Interpretation 26

4. Dimensional Results 26

4.1 Introduction 26

4.2 Rescaling the Dimensionless Model 27

4.3 Input Parameters 28

4.4 Base Example 30

4.5 Preliminary Basaltic Examples 31

4.5.1 Basaltic Conclusive Remarks 33

4.6 General Examples 34

4.7 Extreme Examples 35

5 Discussion 36

5.1 Introduction 36

5.2 Crystal Settling 36

5.3 Implications for the Rheology of Magmas 38

5.4 Effect of Bubbles 40

5.5 Effect of Non-Spherical Crystals 41

5.6 Effect of Unsteady Conditions 43

6 Conclusion 43

7. References 46

8. Appendix 54

1 Introduction

In the current age of volcanology, much is known about magma storage regions from petrological and geochemical methods, such as geothermobarometry (Brey & Köhler, 1990).

The physics of the volcanic eruption process is also well understood from monitoring and observation of natural volcanic eruptions themselves. However, the flow processes that occur within the volcanic conduit between the magma chamber and the Earth's surface are poorly understood due to a lack of direct experimentation methods.

Limited experimentation methods exist to collect this form of data, with what is currently understood about conduits predominantly coming from the results of numerical modelling. Also, conclusions are often drawn from field observations of magma samples and xenoliths by examining the flow patterns in these samples (Gilbert & Lane, 2008). Many previous studies attempt to explore a wide range of physical and compositional effects that also result from a large range of physical properties. For example, these properties include: variable conduit geometries, magma types, temperature changes, etc. Consideration of all these effects leads to an increase in model complexity (Spiegelhalter, et al., 2002) when attempting to accurately simulate a natural volcanic eruption.

When investigating the consequence of changing one parameter on the system, it is not practical to include all these variables. Hence, these models tend to come under one of two types; steady or unsteady states (Rodgers, et al., 1991). A steady state model is one that does not vary with time. In other words, the constitutive equations do not have a time dependence component (Slezin, 2003). This enables the model to be simplified in a way that assumptions about the time dependence components may be used to see how the model varies spatially etc. The model utilised in this dissertation, as described in the next sections, takes the form of a steady state to enable these assumptions to be made.

1.1 Background physics

Throughout this dissertation, the liquid melt phase of the magma is assumed to have a Newtonian rheology, which is a reliable assumption to take following earlier research (Ryerson, et al., 1988). The presence of solid crystals suspended in this melt is widely assumed to give rise to a non-Newtonian rheology of the magma (Caricchi, et al., 2007). This has strong implications for the behaviour of the magma itself and hence for the processes occurring in the conduit. For example, during magma ascent, it is widely assumed that strain partitioning occurring at the walls results in a shear-thinning and flow localisation of the melt and crystal suspension (Ishibashi, 2009). This comes from an a priori knowledge following the findings of non-Newtonian rheology, however the precise reasons for this rheology occurring in magmatic systems themselves is still debated in volcanology.

However, previous works on flow localisations of particles in cylindrical channels and pipes have proven that local changes in the particle volume fraction result from the effect of particle migration away from the walls of the pipe. This lateral migration is induced by mechanical interactions between particles when they are sheared in suspension in a fluid. This creates a grain dispersive pressure across the width of the flow (Komar, 1972).

Figure 1.1 removed for copyright

This figure is from Komar (1972), so it isn't reproduced in this online version. Please see the original paper.

Figure 1.1*: Changes in concentration of crystals in two examples.* ***a*** *shows Olivine phenocryst over the half width of the dyke and* ***b*** *is the size sorting over the full width of another example dyke, taken from Komar, 1972.*

The extent to which this phenomenon occurs is most strongly dependent on the particle concentration in suspension, with a higher initial volume fraction resulting in a more pronounced effect (Lecampion & Garagash,

2014).

During flow, the velocity gradient must be constant across the width of the pipe. Hence, in order to maintain this grain dispersive pressure in the radial direction, the concentration of particles must decrease towards the walls to offset the increase in flow velocity gradient in the centre of the pipe (Komar, 1972). This is visualised in a magmatic dyke setting in Figure 1.1, with the graph in *a* showing an increasing concentration of crystals towards the centre of the dyke and *b* showing the size of crystals increasing at the centre of the flow also. It is important to note that this dissertation only considers a polydisperse suspension of crystals and melt, so the outcome of size sorting is only speculated upon.

1.2 Initial Applications to Magmatic Systems

Previous studies such as Barrière, 1976 attempted to make the first application of the early concept of crystal migration to magmatic systems. In that study, three processes are outlined; the Bagnold, Wall and Magnus effects. A combination of these act to explain the physics behind the crystal migration process. Following subsequent studies, these ideas have largely been rendered redundant, however this same theory has formed the basis for more recent works in this topic and aiding conceptualisation in this dissertation.

In Lecampion & Garagash, 2014, the process of particle migration is driven by a particle pressure acting on each individual particle, as a result of collisions between neighbouring particles. This produces an overall movement of these particles away from the conduit margins towards the centre of flow. This is considered to be the same process as the Bagnold Effect, but with more rigorous mathematics behind it. The effects of the other two, Magnus and Wall, become increasingly less important as initial crystal volume fraction

increases and so are not considered any further. Further description of the Lecampion & Garagash, 2014 model is given in later sections of this dissertation.

These earlier papers appear to suggest that these effects are possible in magmatic systems, although no physical basis for the models described in these past studies has yet been put forward. The aim of this dissertation is to use the model described in Lecampion & Garagash, 2014 with the aid of these previous models to evaluate the extent to which this phenomenon of crystal migration is occurring in a volcanic conduit. A forward modelling technique is applied here to generate synthetic data for the dispersion of the crystal volume fraction in a conduit, after which calculations of other physical parameters can be undertaken.

It is important to note that this is the first rigorous mathematical application of the theory of crystal migration to magmatic systems. The method of forward modelling in this research does not assume any a priori information of non-Newtonian magma rheology, allowing this concept to be tested alongside investigating crystal migration.

1.3 Field Evidence

Field observations of exposed ancient volcanic dykes often show a higher concentration of phenocrysts in the centre of the dyke itself, compared to the walls. Earlier studies investigating these observations considered the phenomenon of crystal migration to be responsible for this pattern (Komar, 1972). However, this theory would suggest that the dyke is filled with a single flow of magma, which stops when it reaches the furthest extents of the dyke geometry.

In reality, this is not the typical emplacement mechanism for magma in dykes. Typically, the flow moves continuously through the dyke and stops only when the magma is cool enough to solidify and block the path of further flow (Bruce & Huppert, 1990).

When the magma is emplaced, the ***a*** edge of the flow at the walls cools faster than the centre (Petford, et al., 1994). As time continues, the radius of the flowing portion in the dyke decreases in size, shrinking from the peripheries, as the magma continues to cool inwards, as seen in Figure 1.2a. Hence, the radius of flow gets smaller as it cools further, giving the effect of more crystals being present in the eventually solidified magma towards the centre. This is due to the same number of crystals being present in the smaller dyke volume of this constricted flow, hence giving the impression of an increase in concentration. (Correy, 1988). Figure 1.2b is included to show that the opposite effect is possible, with the flow width increasing in diameter due to meltback, although this process is not considered further in this dissertation.

Figure 1.2 removed for copyright

This figure is from Bruce & Huppert (1990), so it isn't reproduced in this online version. Please see the original paper.

Figure 1.2a-b*: Schematic diagrams of* ***a*** *development of blocking via solidification and* ***b*** *development of meltback through channel melting, taken from Bruce & Huppert, 1990.*

After this discovery, the phenomenon of crystal migration was largely discounted as a naturally occurring effect. However, in the case of a largely silicic volcanic conduit, cooling and inward growth of the solidified magma at the periphery of the flow does not occur, as magma across the whole width of the conduit is continually replaced by new hotter magma (Blake & Campbell, 1986). With this information, the basis of this dissertation can be formulated around the assumption that crystal migration is possible in volcanic conduits. One

avenue for investigation here is to investigate the extent to which crystal migration may be present in volcanic conduits of differing magma compositions.

1.4 Objectives & Hypotheses

This dissertation aims to answer the following questions surrounding the application of crystal migration to a magmatic setting.

Several questions to be investigated include:

1. To what extent does crystal migration occur within a natural magmatic setting?
2. What are the effects on the results when the assumptions used in the calculations are challenged?
3. What does this mean for the rheology of the magma if crystal migration is or is not occurring?

A hypothesis to be tested throughout this dissertation is that: "*The particle pressure acting on the crystals in magmas can be relevant under natural conditions*". This hypothesis is relevant as the particle pressure acting on the crystals is what drives the crystal migration process. In other words, it states that crystal migration is a process that can be achieved under natural conditions. This will be tested from investigating the output of the code to see the extent to which crystal migration is occurring in under the defined natural conditions.

1.5 Relative Importance

This research is important as crystal migration has largely been neglected as a naturally occurring phenomena due to the reasons described above. This has led to the omission of the potential effects of crystal migration in many numerical models and may have

resulted in misinterpretation between the models produced and the real scenarios. The results of this dissertation may help in the understanding of magma flow processes in volcanic conduits and may go towards the improvement of numerical models aiming to simulate those processes.

2 Background and Methods

2.1 Introduction

As stated, the aim of this dissertation is to investigate the extent to which crystal migration is present and occurring in different volcanic settings. This will take the form of a modelling approach that seeks to make the first application of the physical model of Lecampion & Garagash, 2014 to that of a magmatic system. This will be achieved by utilising a numerical simulation of this model, coded by Dr. Vasseur, to describe crystal migration for the case of a pressure driven magma flow. In order to make this application, the model must first be described for the case of particles in a pipe.

2.2 Model Description

The classical view of suspensions comprises an effective viscosity of both the particles and fluid (Stickel & Powell, 2005). Boyer, et al., 2011 aims to more accurately describe the dynamics of a suspension by considering a frictional rheology between suspended particles, as well as hydrostatic components. In that study, mathematical laws to express the friction coefficient are developed including the frictional and hydrostatic components weighted accordingly.

It is important to note that as the particle volume fraction is increased, the hydrodynamic interactions become less important and the direct particle contacts become

more prevalent in the rheological response (Guazzelli & Pouliquen, 2018). Also, if no crystals are present in the magma, the velocity profile across the conduit in the radial direction would show that of perfect Poiseuille flow (Yamato, et al., 2011). The examples used in this dissertation all contain a quantity of crystals in suspension, so a deviation from this flow profile is to be expected.

2.2.1 Cartesian vs Cylindrical

It is important to note that throughout this study, cylindrical coordinates are used to simulate the models described. This is appropriate as many of the examples used here are of silicic magma types, in a volcanic conduit, with cylindrical coordinates more appropriate for conduit geometry. This model can also be realised using cartesian coordinates, however this is less accurate for the examples described here. In cylindrical coordinates, the axial (i.e. vertical in the case of a volcanic conduit) and radial directions are hereafter denoted as z and r respectively.

2.2.2 Applied Rheology and Viscous Number

Boyer, et al., 2011 acts to phenomenologically describe the rheology of the suspension with a viscoplastic frictional rheology. Equations 2.19 and 2.20 in Lecampion & Garagash, 2014, labelled as equations 2.1 and 2.2 in this dissertation, analytically describe the

$$\mu(\phi) = \mu_1 + \frac{\phi_m}{\beta}\left(1 - \frac{\phi}{\phi_m}\right) + \left(I(\phi) + \left(\frac{5}{2}\phi_m + 2\right)I(\phi)^{\frac{1}{2}}\right)\left(1 - \frac{\phi}{\phi_m}\right)^2 \quad \textit{Equation 2.1}$$

dependence of the frictional coefficient μ on the particle volume fraction ϕ and dimensionless viscous number I. These equations allow for the friction coefficient to be calculated for any particle volume fraction in the suspension.

$$I(\phi < \phi_m) = \left(\frac{\phi_m}{\phi - 1}\right)^2 \text{ and } I(\phi \geq \phi_m) = 0 \qquad \textit{Equation 2.2}$$

This friction coefficient develops from the constant value $\mu_1 = 0.3$ at the 'jamming limit' of $I = 0$ of a dense suspension – as seen in the second equation of 2.2. The constant of $\phi_m = 0.585$ corresponds to the maximum solid volume fraction of spherical crystals, termed the 'jamming value', with $\beta = 0.158$ acting as a 'compressibility' coefficient.

2.2.3 Origin of Viscous Number from Inertial Number

The origin of this dimensionless viscous number is from Boyer, et al., 2011. An inertial number I_n is defined as the ratio between the inertial time of particle rearrangement, $t_{micro} = d\sqrt{\frac{\rho_p}{P^p}}$ and time of strain, $t_{macro} = \frac{1}{\dot{\gamma}}$, giving $I_n = \dot{\gamma} d\sqrt{\frac{\rho_p}{P^p}}$. This case is assuming hard spheres with diameter d, density ρ_p and confining pressure, P^p. These equations are suitable in the examples of dense granular suspensions in pipe and channel flow, the concept of which is adopted in this dissertation. For the case of a low Stoke's number, viscous scaling can be applied due to viscous forces becoming the dominant response at the particle interaction scale, hence $t_{micro} = \frac{\eta_f}{P^p}$. This leads to the conversion of the inertial number I_n to the new dimensionless viscous number $I = \frac{\eta_f \dot{\gamma}}{P^p}$ (Boyer, et al., 2011). The variation of the friction coefficient, μ and the particle volume fraction, ϕ as a function of this dimensionless viscous number can be seen in Figure 2.1. This figure shows the data collapsing onto the single curves, used to determine the constants of maximum packing fraction, ϕ_m and friction coefficient, μ. These graphs therefore show the importance of the dimensionless viscous number, I in relation to the process of particle migration.



Figure 2.1*: Figure taken from Boyer, et al., 2011 to show the relationship of the friction coefficient, μ (top panels) and particle volume fraction, ϕ (bottom panels) both as a function of the dimensionless viscous number, I (labelled I_v in this figure) for each case of (a) and (b) of linear and (c) and (d) of semilogarithmic scales.*

It stands that if the dimensionless viscous number, I is much less than a value of one, there will be migration of crystals, or in other words; $I << 1$. By contrast, if I is much larger than a value of one, $I >> 1$, crystal migration will not be present in the system. This concept is visualised in Figure 2.2 below.

2.2.4 Continuum Model

This frictional rheology construct is embedded into an overlying continuum model for the case of a suspension in a pipe. It is this continuum model that solves for the phase

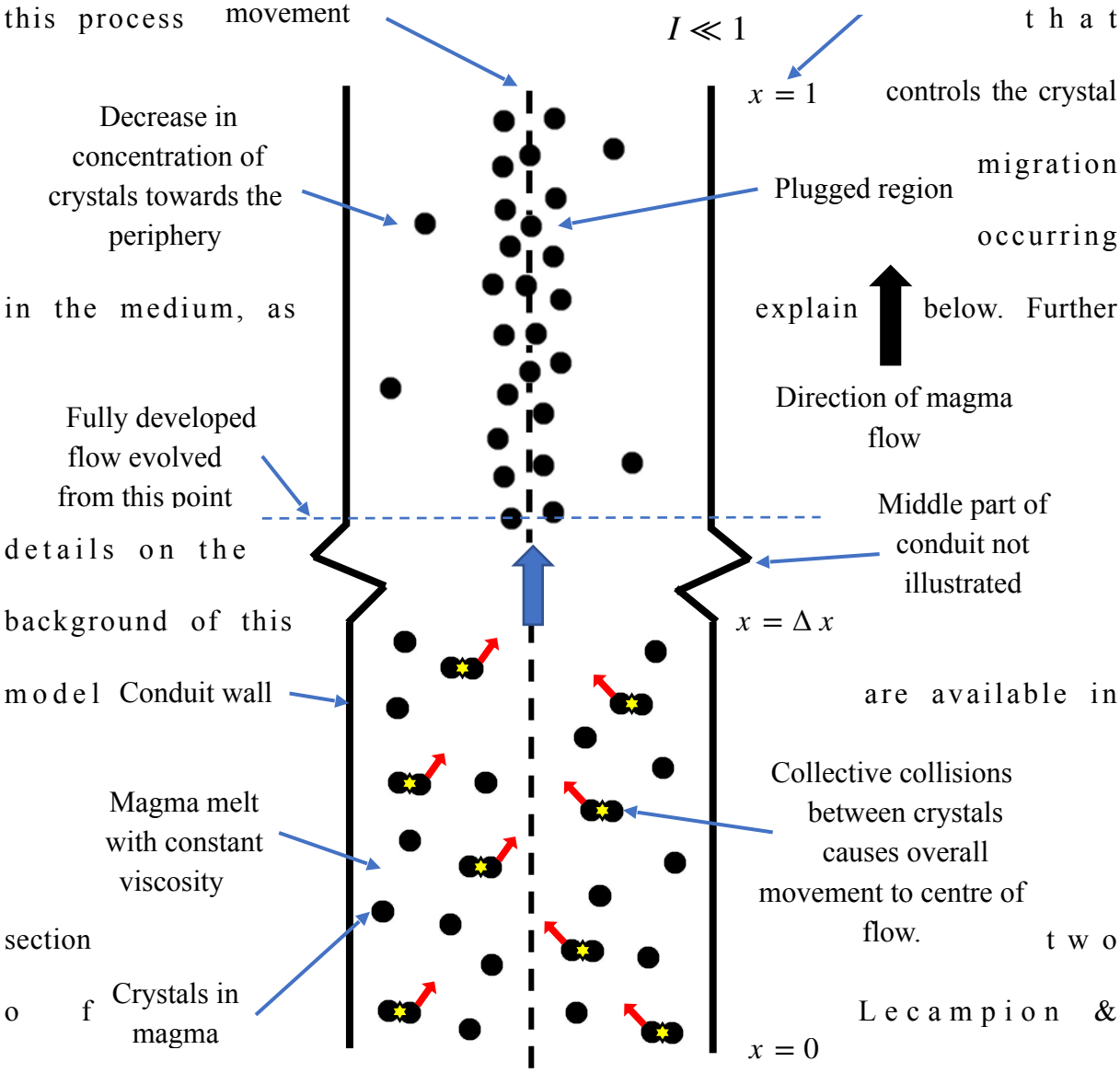


***Figure 2.2**: Schematic image illustrating the concept of crystal migration due to high shear at the conduit walls creating high strain to move crystals towards the centre of flow. Low shear in the centre of flow results in no lateral movement of crystals.*

Garagash, 2014, but a brief description is given here.

Equation 2.1 leads to crystal migration as the continuum model is solving for the shear stress, τ and particle normal stress, σ_n' using the friction coefficient, as described in equation

$$\mu = \frac{16\ \tau}{-\sigma_n'} \qquad \textit{Equation 2.3}$$

2.3 (Boyer, et al., 2011). Note the negative sign is following the convention of negative stress as compressional.

It is this particle pressure that arises from a shear stress and frictional interaction between particles and fluid, induced by the fluid moving relative to the fixed walls. This means that when the particle pressure is high, there will be a movement of particles away from these regions of higher pressures at the walls towards the region of lower pressure at the centre of the flow. This concept is also visualised in Figure 2.2.

2.2.3 Numerical procedure

From this point onwards, all parameters introduced have been rendered dimensionless, chosen for this description of the model. The numerical procedure for solving particle migration in the case of a pressure driven suspension is initiated by the entrance conditions, namely, the values the physical parameters take at the start of the pipe. Fundamentally, the model uses the initial particle volume fraction, ϕ_0 as the uniform entrance condition for ϕ to calculate the entrance condition values for the other variables. The flow at the entrance is assumed to follow a perfect Poiseuille flow which then transitions to plug flow, due to the forces acting on the particles as it is sheared. In cylindrical coordinates this is:

$$v_x = \left| \nabla p_0 \right| \frac{I_0}{\mu_0} \frac{1 - r^2}{4} \qquad \textit{Equation 2.4}$$

$$-\sigma_n' = \frac{\left| \nabla p_0 \right| r}{2\mu_0} \qquad \textit{Equation 2.5}$$

Where μ_0 and I_0 are calculated from equations 2.1-2.2. The initial radial flow velocity is assumed to be zero, i.e. $v_r = 0$. Given the gap-average entrance velocity value

$$\left| \nabla p_0 \right| = \frac{8\mu_0}{I_0} \qquad \textit{Equation 2.6}$$

$v_0 = \langle v_z \rangle = \int_0^1 v_z dr = 1$, the mean pressure gradient may be derived from equation 2.4 to give:

The calculations are undertaken in the code by setting out a staggered grid to set up the numerical space with the axial direction divided into N_z intervals with each step of size dz and the radial direction divided into N_r intervals with each step having size $dr = \frac{1}{N_r}$. The procedure steps described in the next sections are then used to advance the solution from z to $z + dz$, which is continually repeated until the top of the channel is reached for $z = N_z dz$.

2.2.5 Steady State Flow to find Particle Pressure

Equation 5.2 in Lecampion & Garagash, 2014 can be re-written assuming a steady state flow – where the solution does not vary with time, hence $\frac{\partial \phi}{\partial t} = 0$. In Cylindrical coordinates this is equation 2.7:

Which $\frac{\partial \sigma_n'}{\partial z} = -\frac{1}{r}\frac{\sigma_n'}{S v_z}\frac{\partial}{\partial r}\left(\kappa \frac{\partial}{\partial r}\left(r\sigma_n'\right)\right) - \frac{v_r}{v_z}\frac{\partial \sigma_n'}{\partial r} + \sigma_n'\left(\frac{\partial \left|\nabla p\right|}{\partial z} + \frac{1}{r}\frac{v_r}{v_z}\right)$ may be solved to find σ_n' with a BTCS (Backward-Time, Centred-Space) finite-difference numerical scheme, coupled with a relaxed fixed-point iteration method. This is assuming a boundary of symmetry at $r = 0$, such that $f = \left(1 - \phi\right)^{\alpha}$ $f = \frac{1-\phi}{1 + \frac{4.6\phi}{(1-\phi)^3}}$ $f = \frac{(1-\phi)^3}{10\phi}$ *Equation 2.8*

$\frac{\partial \sigma_n'}{\partial r} = 0$ and $\sigma_n' = 0$ at $r = 1$. For Stokesian flow, the scaled permeability, κ may be calculated from equation 2.8:

Where $f(\phi)$ is a hinderance function. Here the simple form proposed by Richardson & Zaki, 1954 is used: $f = (1 - \phi)^{\alpha}$ for which $\alpha = 5.1$ (see Figure 1 in Lecampion & Garagasg, 2014). The inelastic storage coefficient, S is given by:

$$S = -\frac{\mu}{\phi}\frac{d\phi}{d\mu} \qquad \textit{Equation 2.9}$$

2.2.6 Mean Pressure Gradient

Once the above step is complete, the mean pressure gradient may be computed with the global continuity condition $\langle v_z \rangle = 1$ of which the gap-averaged velocity may be $v_x = -\int_0^1 \sigma_n' I r^2 dr$ given by: *Equation 2.10*

As I itself is a function of the mean pressure gradient, this equation may be solved for $|\nabla p|$ by using the following sub-iterative procedure:

$$|\nabla p|_{next} = \frac{1}{\langle v_x \rangle_{prev.}} |\nabla p|_{prev.} \qquad \textit{Equation 2.11}$$

Where subscripts $next$ and $prev.$ refer to the successive sub-iterations of $|\nabla p|$ and $\langle v_x \rangle_{prev.}$ are given by the previous equation when evaluated at $|\nabla p| = |\nabla p|_{prev.}$

2.2.7 Strain Rate, Particle Volume Fraction and Flow Velocity

The shear stress is now able to be calculated from $\tau = \frac{1}{2}\left|\nabla p\right| r$, using $\left|\nabla p\right|$ from the previous step. This in turn means the friction coefficient itself may be determined from equation 2.3 and hence extract the particle volume fraction by solving equation 2.1 for ϕ. It is also important to note that the shear rate may be determined using $\dot{\gamma} = -\sigma_n' I$. Lastly, the axial velocity is determined from numerical integration of the following:

$$\frac{\partial v_z}{\partial r} = \sigma_n' I \qquad \textit{Equation 2.12}$$

And the lateral velocity from numerical integration of:

$$\frac{\partial}{\partial r}\left(r v_r\right) = \frac{\partial}{\partial r}\left(\kappa \frac{\partial}{\partial r}\left(r\sigma_n'\right)\right) - \frac{\partial v_z}{\partial z} \qquad \textit{Equation 2.13}$$

2.3 Outputs

Figure 2.3 shows the normalised results of the Lecampion & Garagash, 2014 study to visualise the evolution of the flow in a channel. These results are normalised by scaling of the radial distance r by the radius R and in the axial direction z by the development length scale $L = R^3/a^2$ (Nott & Brady, 1994). It is clear to see that in all cases there is an increase in solid particle volume fraction towards the centre of the flow. This becomes more pronounced as the initial solid crystal volume fraction, ϕ_o increases. This is to be expected following the migration of crystals away from the walls towards the centre of flow, forming a plugged region, centred around zero radial position (Komar, 1972).

3. Dimensionless Results

3.1 Introduction

This section presents the output of the model described in the previous section from Lecampion & Garagash, 2014, for the case of hard spheres in an incompressible liquid. The model is made dimensionless whereby each quantity is divided by a corresponding kinematic scale, each defined as equations $3.2 - 3.4$ from Lecampion & Garagash, 2014. The outputs achieved in this section give the basis for the dimensional model in the next section that will be applied to a magmatic setting. Volcanic terms are used in this section to give a clearer understanding of this application and reducing confusion when going between Lecampion & Garagash, 2014 and this dissertation.

Figure 2.3 removed for copyright

This figure is from Lecampion & Garagash (2014), so it isn't reproduced in this online version. Please see the original paper.

Figure 2.3*: Figure taken from Lecampion & Garagash, 2014 to show the development of flow in a pipe with axial direction z (labelled as x in this figure) and radius* R *from three different initial particle volume fractions;* ϕ_o

3.2 Scaling Parameters

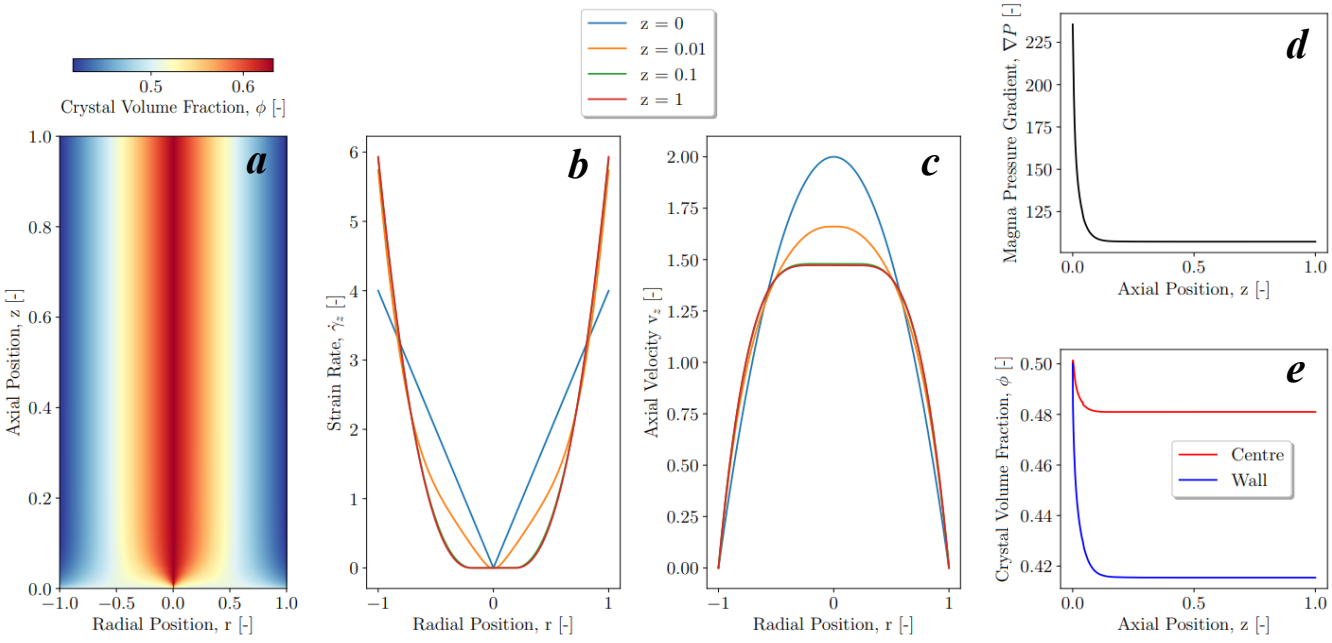
Scaling of the physical parameters used in the model is required following the assumption that the relative phase flux is more functional across the channel rather than along it. However, it must be maintained that the axial velocity is much larger than the velocity across the channel. The 'kinematic scales' seen as equations 3.3a – 3.4 in Lecampion & Garagash, 2014 are used as the scaling factors for this conversion. This non-dimensionalisation is undertaken by dividing each quantity by its respective scaling parameter, given from Lecampion & Garagash, 2014.

The scaling factor known as the 'aspect ratio' $\delta = R/L$, where R is conduit radius and L is axial length, is used when converting the initial velocity into the axial and perpendicular components. To convert the inlet velocity into a velocity in the radial direction, this scaling factor is multiplied by the inlet velocity value.

The gap averaged crystal volume fraction $\langle\phi\rangle$ is calculated for two positions in the radial direction; the first at the centre of the flow $\phi(r = 0)$ and the second at the wall of the conduit $\phi(r = 1)$ to see the changes in this quantity with respect to position. An example of this can be seen in Figure 3.1e.

3.3 Results

Figure 3.1a-e shows the dimensionless model generated from the code. Each figure is described separately, and the effects of crystal migration are explained in all cases.



***Figures 3.1a-e**: Figures produced of dimensionless case as output of code from this study. From left to right; **a** is the crystal volume fraction plot for the conduit space, **b** is the axial strain rate along the conduit, **c** is the axial velocity along the conduit, **d** is the magma pressure gradient along the conduit and **e** is the crystal volume fraction value for both the centre and wall of the flow.*

3.3.1 Particle Volume Fraction Concentration

Figure 3.1a displays an increasing concentration of the crystal volume fraction, ϕ towards the centre of the conduit at $r = 0$ at all length values $z > 0$ along the conduit. This therefore shows crystal migration must be occurring due to a higher concentration of crystals at the centre of the flow, decreasing towards the walls. This is consistent with the result seen in Figure 2.3.

3.3.2 Strain Rate vs Radial Position

The strain rate in the axial direction, $\dot{\gamma}_z$ shown in Figure 3.1b increases rapidly as the walls on either side of the conduit are approached. This rate of increase is also seen to increase more rapidly for lengths further along the conduit. A higher strain rate at the periphery of the flow results in a higher shearing force exerted from the walls to the suspension, resulting in a more pronounced grain-dispersive pressure (Komar, 1972). This in turn results in a faster onset of fully developed flow as particles are forced away from the margins towards the centre of flow at a quicker rate. The strain rate does not change for axial length values of $z > 0.1$, suggesting no further lateral movement of crystals beyond this point. Hence, this gives direct evidence that crystal migration must be occurring in Figure 3.1b, as fully developed flow has been achieved due to no further rearrangement of crystals.

3.3.3 Axial Velocity vs Radial Position

Figure 3.1c shows the axial velocity of the flow, v_z as a function of the radial position. This curve starts as a perfect parabola as soon as the magma is entered into the conduit, however for further distances up the conduit, it evolves to be become less parabolic in shape and more like a ‘plug’. This is the result expected from Figure 3.2, with this phenomenon becoming more pronounced for increasing initial crystal volume fraction. So, the fact that the

velocity profile becomes plug shaped in Figure 3.1c gives good evidence for particle migration occurring in this setting.



***Figure 3.2**: Figure taken from Lecampion & Garagash, 2014 to illustrate the evolution from Poiseuille to plug flow, in terms of the axial velocity in a slot with half-width H. this is shown for different initial particle*

3.3.4 Magma Pressure Gradient vs Axial Position

The magma pressure gradient, ∇P along the axial length of the conduit in Figure 3.1d is shown to rapidly decrease and plateau to a constant value of approximately 100. This is the case from $z > 0.1$ onwards, with no change in the magma pressure gradient above this point, suggesting that fully developed flow has occurred here. This is the case as would be expected from Figure 3.3, where the total magma pressure gradient plateaus into a constant value for each of the initial particle volume fractions used. This also gives evidence for crystal migration as it suggests no re-organisation of crystals is

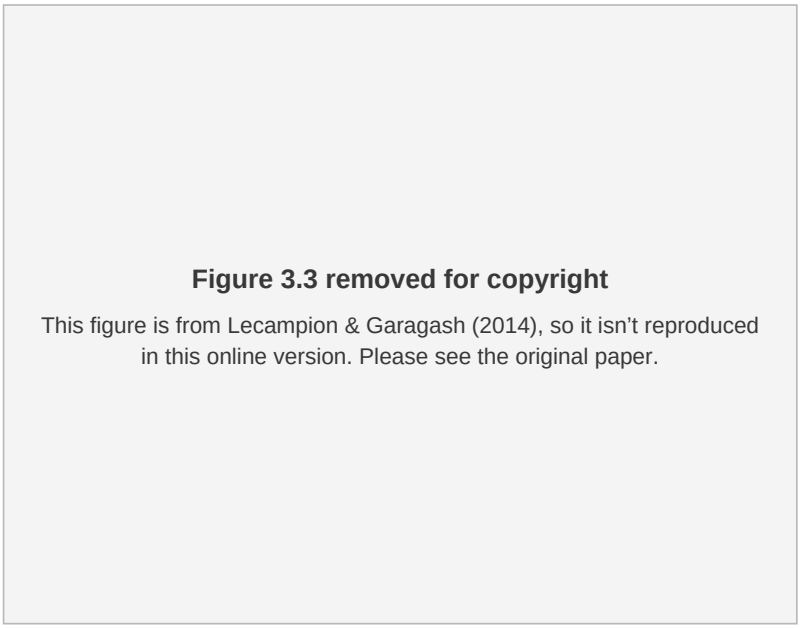


***Figure 3.3**: Figure taken from Lecampion & Garagash, 2014 to show the development of the total mean pressure gradient with increasing axial distance (labelled as x in this figure) from the channel 'slot' (solid line) or pipe (dashed line) entrance. The trend is calculated for increasing values of the initial solid particle volume fraction, ϕ_o.*

occurring in the flow from this point onwards, so no changes in particle pressure are experienced.

3.3.5 Gap Averaged Crystal Volume Fraction vs Axial Position

Finally, in Figure 3.1e the crystal volume fraction along the axial length of the conduit shows a rapid decrease to a plateau at both the centre of the flow and the wall value. However, a significantly more rapid decrease occurs for the wall value compared to at the centre.

Figure 3.4 acts to illustrate the development of the wall and the gap average values of the particle volume fraction as the axial length of the flow increases. The fact that a constant

Figure 3.4 removed for copyright

This figure is from Lecampion & Garagash (2014), so it isn't reproduced in this online version. Please see the original paper.

Figure 3.4*: Figure taken from Lecampion & Garagash, 2014 to show the development of the particle volume fraction at the wall and the gap averaged value across the flow for both channel and pipe flow as solid and dashed lines respectively. Results shown are that of* $\boldsymbol{a}$ $\phi_o =$ *0.05, 0.2, 0.4, 0.55 and* $\boldsymbol{b}$ $\phi_o =$ *0.1, 0.3, 0.5.*

value is achieved at both the wall and centre, suggests that particles are no longer migrating away from the walls as the suspension approaches the top of the conduit. Also, the fact that the ϕ is higher at the centre of the flow, as opposed to at the periphery is significant as it shows a higher concentration crystal volume fraction away from the walls, as would be

predicted by particle migration. Fully developed flow is therefore evidenced by these lines reaching a constant value as the axial length of the flow increases.

3.4 Interpretation

It is clear that in the case of Figure 3.1a-e, the onset of fully developed flow occurs soon after the crystals are intruded into the volcanic conduit, with fully developed flow achieved from $z \geq 0.1$. This is evidenced from all Figures of 3.1a-e from the reasons described above.

Now that particle migration is proven to occur under the conditions set for the case of Figure 3.1, it now remains to be tested if this phenomenon of particle migration is able to occur in magma flow. For this example, the particles that would migrate are the crystals held in suspension of the liquid melt.

The afore-mentioned models may be applied to a magmatic system as the components of magma and conduit geometry can be approximated to the constituents of those models.

4. Dimensional Results

4.1 Introduction

In the previous section, it was seen that particle migration is possible under the dimensionless, normalised quantities. However, in order to have practical value, the normalised results of this study must be converted into dimensional quantities and applied to a magmatic setting to test the hypothesis and assess if crystal migration in magma is possible under natural conditions.

To apply this model to real world examples, the now dimensional quantities are multiplied by the corresponding scalar values of each quantity for a particular case study. This

conversion process, between a generic dimensional model to a real-world example, requires the full suite of input parameter values to be known. Each of these values control to a greater or lesser extent, the degree of organisation of particles in the suspension. Hence, no firm conclusions about crystal migration in volcanic conduits can be drawn before this conversion is undertaken in full.

In the natural world, magma compositions lie on a continuum from broadly mafic to broadly silicic. From this, the magma can be divided up further into basaltic, andesitic and dacitic types (Middlemost, 1994). The approach taken in this section is to define the most likely case study locations on Earth where crystal migration may be possible and use these in the dimensional model to test the hypothesis. This means the extent to which crystal migration is occurring can be seen as a function of varying volcanic setting.

4.2 Rescaling the Dimensionless Model

Constitutive laws in Lecampion & Garagash, 2014 are described as "incrementally akin to Newtonian fluid", so classical Newtonian lubrication scaling is used to scale the normalised quantities into dimensional space (Frigaard & Ryan, 2004). The conversion is achieved by multiplying the dimensionless quantities by the corresponding scaling factor seen from equations 3.2-3.4 in Lecampion & Garagash, 2014; the opposite process to that when making the model dimensionless.

For the axial length of the flow to be converted into dimensional conduit length, this normalised vector z with values between zero and one, must be multiplied by the 'length scale', calculated from $L = R^3/a^2$ (Nott & Brady, 1994), with a as the crystal size in meters. In this case, L represents the length of conduit required for fully developed flow of the magma suspension to develop. It is important to point out that this distance may be much

larger than the actual length of conduit for any case study, in which case fully developed flow will not be achieved before the magma reaches the surface.

From this equation, it is clear the axial length of conduit required is highly sensitive to the radius of the conduit itself. If the radius is large, the length of conduit required will be very large also. Crystal size has the opposite effect with larger crystals causing the conduit length required to be smaller.

In nature, volcanic conduits tend to vary between 2 km < L_c < 20 km (Cassidy, et al., 2019), so when considering these conduit lengths, only the very bottom part of Figure 3.1a will be realised under natural conditions. If the radius is smaller, and the crystal size is larger, the further up the real case will sit on the model in Figure 3.1a. This can be seen by undertaking first order calculations; for example if the radius used is 20 m and crystal size 10^{-3} m, the axial length of conduit required for fully developed flow is $(20)^3/(10^{-3})^2 = 8 \times 10^9$ m. Whereas, taking a smaller radius of 10m and larger crystal size of 10^{-2} m, $(10)^3/(10^{-2})^2 = 1 \times 10^7$ m, hence results in a shorter length required. This is significant as it limits the range of input parameters that can achieve fully developed flow to smaller conduit radii and larger crystal sizes. Case studies that do not meet these conditions can be expected to not reach fully developed flow during the length of their conduit. Dimensional case studies will now be tested using this model to investigate which case studies this applies to or not.

4.3 Input Parameters

The input parameters for each chosen example are found from a literature review of past studies carried out on these volcanoes. All input values for each example can be seen in Tables 7.2-7.8 in the Appendix section. The associated references for the origin of each of

these values is also included. Where values cannot be found from previous studies, values for conduit length and crystal volume fraction are taken from Figure 4.3 for each example displayed. Table 4.1 is included as an example to show the inputs used in the code for the Base example.

Example	Property	Value	Unit
Base	Conduit Length	5000	m
	Crystal Content	0.5	-
	Water Concentration	3	wt %
	Glass Composition	-	-
	Viscosity	100.00	Pa s
	Conduit Radius	5	m
	Temperature	1090	^{o}C
	Crystal Size	0.01	m
	Crystal Density	2700	kg m^{-3}

Table 4.1: *Input parameters used in the code to generate the figures seen in figure 7.7 for the Base Example. The property, value and unit is included to give a comprehensive understanding of the origin of the figures produced.*

The viscosity of the magma for each example is calculated from Giordano, et al., 2008 by inputting the relative abundances of the compositions of constituent element oxides into equations 2 and 3 from that study to obtain the values for three constants, named *A*, *B* and *C*. These constants are then inputted into equation 1 to give the viscosity of the magma in the form $log_{10}\eta$. When this value is put in the exponent of the number 10 to negate the logarithm, the value for the bulk viscosity of the magma is achieved. The viscosity also varies significantly with temperature, so the appropriate viscosity is chosen for the specific eruption temperature for each example, determined from Figure 4.3. This process must be repeated for each the different volcanic examples used, due to differences in composition between the magmas.

It is found from Cashman & Giordano, 2014, that in all magma reservoirs feeding volcanoes with a volume much greater than the conduit itself, a reasonably constant and equal

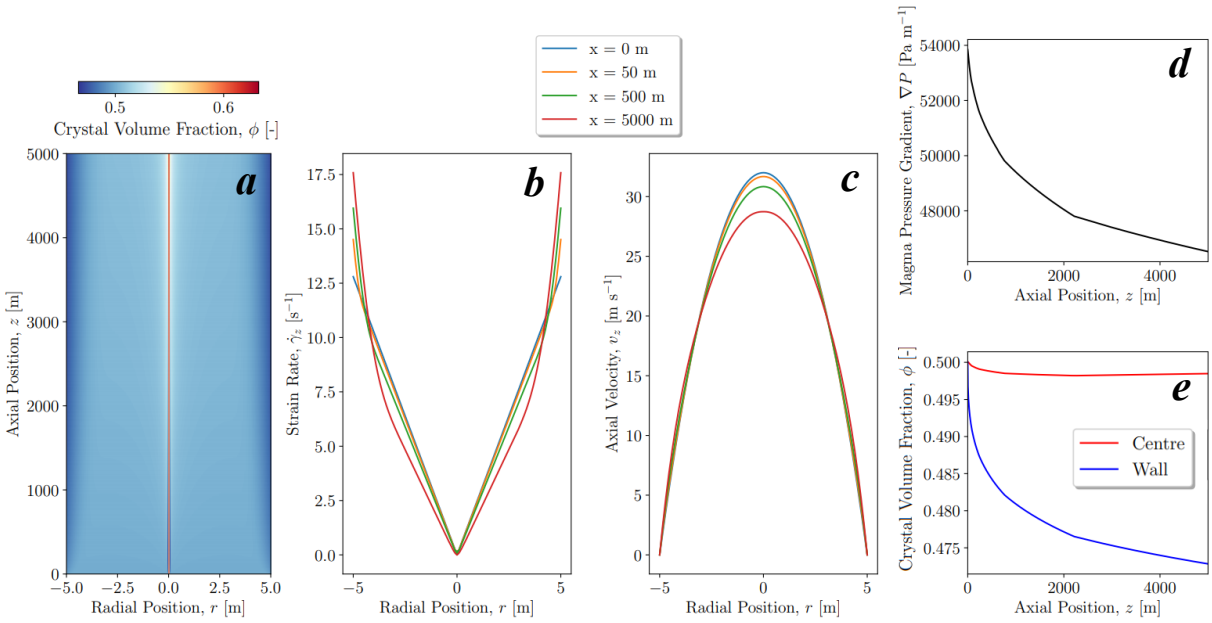
value for the entrance velocity may be assumed. Using this concept, a single inlet velocity at the base of the volcanic conduit may be used for all examples, following this constant value of pressure. Data collated from La Spina, et al., 2021 for use in modelling in that study is used here for the value of inlet velocity to be calculated. These values are the output of the model used in that study. The average value of the inlet velocity is calculated for both Etna and Kilauea to be 12 m/s and 20 m/s, rounded to the nearest integer, respectively. The average of these two velocities is then taken to be 16 m/s and this value is used as the inlet velocity for all dimensional examples in this dissertation.

4.4 Base Example

A 'Base' example is chosen to display the effects of crystal migration in dimensional space. The input parameters are chosen for this example to give the best chance of seeing migration of crystals. This is determined from the reasons described in the previous section.

Crystal migration is clearly evidenced here from Figure 4.1a due to the increase in crystal volume fraction towards the centre of the flow. The other graphs in this figure also show crystal migration following the same explanations given in the previous section.

It is seen in this example that crystal migration is possible in the dimensional space, under these defined conditions, however it is likely that these conditions are not possible in the natural world. This is due in part to the low viscosity of $\eta = 100$ Pas, high crystal volume fraction of $\phi_0 = 0.5$ and small conduit radius of $R = 5$ m, meaning organisation of crystals occurs rapidly. To test if crystal migration is possible in the natural world, real world case study examples are used to fit this dimensional model to see the results.



***Figures 4.1a-e**: Figures produced from the code of this dissertation of the dimensional base example case study, with quantities chosen to give the best chance of seeing crystal migration occurring. From left to right; **a** is the crystal volume fraction plot for the conduit space, **b** is the axial strain rate along the conduit, **c** is the axial velocity along the conduit, **d** is the magma pressure gradient along the conduit and **e** is the gap averaged phi value for both the centre and wall of the flow. Input parameters to produce these figures seen in Table 4.1.*

Due to the symmetries of scaling between dimensionless to dimensional quantities, all plots of b-e will have the same shape and form as each other. With this information, only the crystal volume fraction plot is displayed for each dimensional example from this point onwards.

4.5 Preliminary Basaltic Examples

Basaltic magmas are characterised by both low viscosity and gas content with typically little explosive activity (Green & Ringwood, 1967), allowing easier movement of crystals through the magma. Hence, conduits found in Basaltic volcanoes are a likely candidate for seeing evidence of crystal migration. The downside to this is there is often only a small value for crystal volume fraction, however the influence of this will be tested in this section. Two basaltic case studies are chosen to test this theory: Mt. Etna, Sicily and Kīlauea, Hawaii.

The results of running the code for both Mt. Etna and Kīlauea can be seen in Figures 4.2a and 4.2b for both respectively. It is clear from these figures that crystal migration is not occurring due to the uniform concentration of crystal volume fraction throughout the conduit.

This result can be evidenced further from Figures 7.1a-e and 7.2a-e in the Appendix. Figure 7.1b shows that when the strain rate is plotted against radial position, there is no change observed at any point along the whole length of the conduit. The velocity profile in Figure 7.1c also follows a perfectly parabolic shape at all distances along the conduit, with no change observed for any length along the conduit. The magma pressure gradient in Figure 7.1d does not reach a constant value as would be predicted for fully developed flow. The crystal volume fraction at the wall is seen to decrease significantly faster than that of the centre of the flow, although the decrease seen is very small. This suggests that only a very small number of crystals are preferentially moving away from the walls towards the centre of the flow. Although this is theoretically exhibiting the effect of crystal migration, the number of crystals is so small that this effect is not displayed by any other plot.

The fact that crystal migration is not occurring in either of these examples could have been predicted from first order calculations. For example, the Basaltic example of Mt. Etna has a conduit radius of 25 m from Table 7.2 and an average crystal diameter of 10^{-4} m (Winkler, 1949). Therefore, the length of conduit required for the effects of crystal migration, L is $(25)^3/(10^{-4})^2 = 1.56 \times 10^{12}$ m. From this, it is clear that crystal migration is not possible in the length of conduit at 9000 m for Mt. Etna. When this same calculation is undertaken for Kīlauea, the value for L is $(20)^3/\left(10^{-4}\right)^2 = 8 \times 10^{11}$ m, which is also much larger than the real length of 2000 m. The input parameters for both of these Basaltic studies are given in Tables 7.2 and 7.3 in the Appendix.

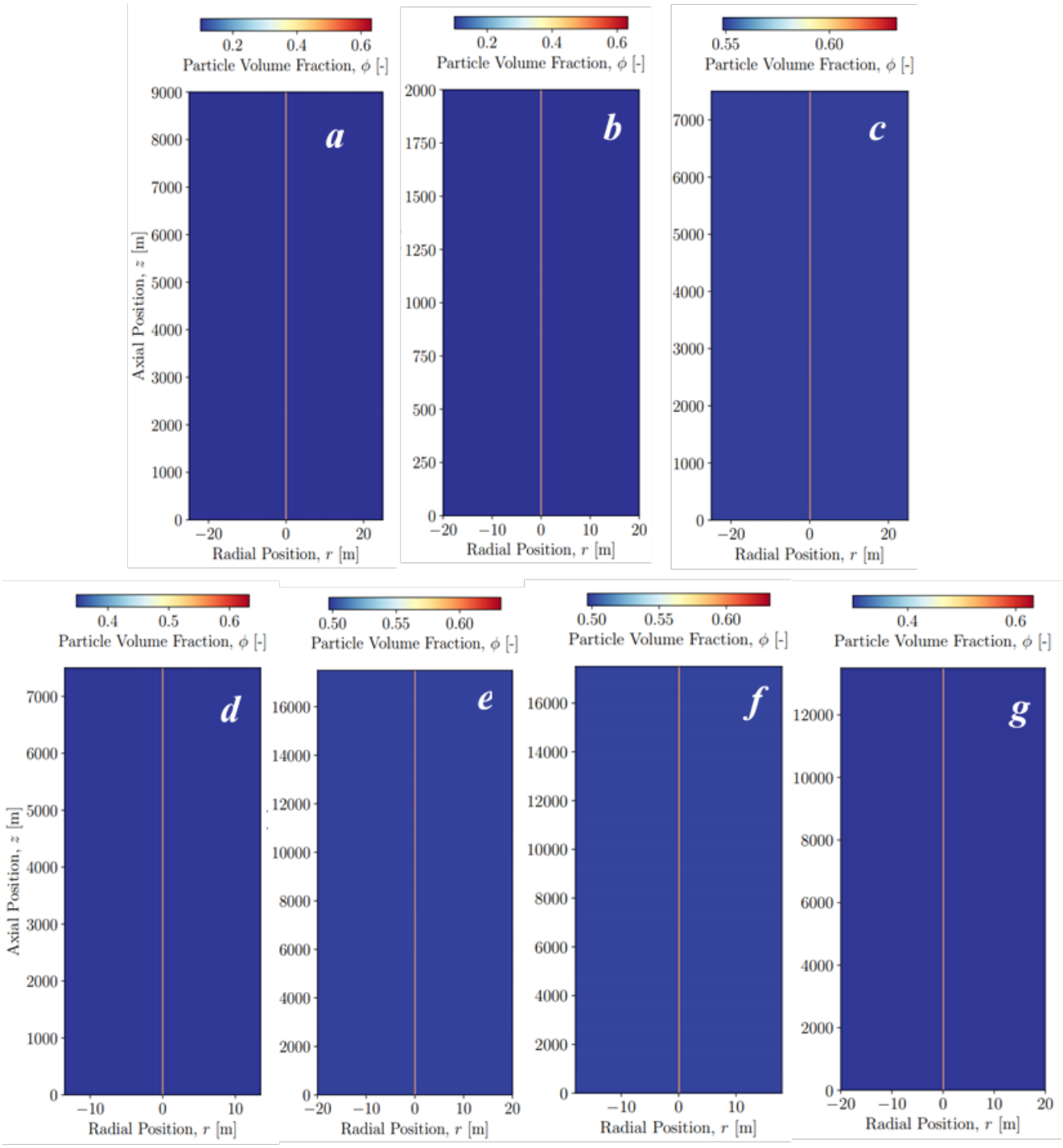


***Figure 4.2a-f**: Cross sections of volcanic conduits of the examples chosen to investigate crystal migration with the concentration of particle volume fraction as a colour scale for **a** Mt. Etna, **b** Kilauea, **c** Unzen, **d** Volcan de Colima, **e** Fish Canyon, **f** Mt. Pelee and **g** Black Butte.*

4.5.1 Basaltic Conclusive Remarks

Neither of these preliminary basaltic examples show the effect of crystal migration. This is due to the input parameters of both these case studies resulting in the length of conduit

required for crystal migration being much larger than the actual lengths of their conduits. For example, the crystal volume fraction used for both these examples is low at $\phi = 0.1$. in the next section, case studies from other volcanic settings will be used in order to see if crystal migration is possible under different magmatic types. From this result, it is speculated that a crystal-rich Basaltic magma would be highly susceptible to crystal migration, however this theoretical magma is rarely realised under natural conditions.

4.6 General Examples

Following the result from the basaltic example, other examples are chosen from Figure 4.3 from Cassidy, et al., 2019 to investigate the extent to which crystal migration is present under different volcanic settings. These examples are ideally chosen based on their proximity to the centre of each group, so as to best represent each magma type. However, there must be a trade off between this and the amount of available literature data for each case

Figure 4.3 removed for copyright

This figure is from Cassidy et al. (2019), so it isn't reproduced in this online version. Please see the original paper.

Figure 4.3a-c*: Graphs from Cassidy, et al,. 2019, showing intermediate magmas plotted as a function of pressure and temperature. The crystal volume fraction for each example is colour coded and depth contours are also marked on each graph. From left to right;* ***a*** *is the Basaltic examples,* ***b*** *is the Andesitic examples and* ***c*** *is the Dacitic examples.*

study. With this in mind, Colima is taken as the Andesitic example and Unzen for the Dacitic example.

The results of both of these examples can be seen in Figures 4.2c and 4.2d for Colima and Unzen respectively. As can be seen from these figures, crystal migration is also not occurring in these locations due to the unifrom concentration of crystal volume fraction in each figure. This is likely due to the high viscosity present in both examples, restricting the movement of crystals through the melt. The full figures can be seen in Figures 7.3a-e and 7.4a-e in the Appendix.

4.7 Extreme Examples

Due to the failure of the case study locations described in the previous sections to exhibit the effect of crystal migration, case studies termed ‘extreme’ examples are used. These extreme examples are chosen from Figure 4.3 for each magma type by having properties that would give the most likely chance of featuring crystal migration. This includes factors such as high crystal volume fraction with a long volcanic conduit, or in other words; a deep rooted magma chamber. From Figure 4.3, Mt. Pelee is taken for the basaltic case, Fish Canyon for the Andesites and Black Butte for the Dacitic case.

The results of each of these examples are seen in Figures 4.2e, 4.2f and 4.2g for Fish Canyon, Mt. Pelee and Black Butte respectively and the full range of graphs can be seen in the Appendix of Figures 7.5a-e, 7.6a-e and 7.7a-e respectively. It can be seen in each of these cases that crystal migration is also not achieved following the uniform crystal volume fraction in each figure. This is significant as it means that there is no location on Earth under a

volcanic conduit setting where crystal migration is possible. The implications for this will be explored in the next section.

5 Discussion

5.1 Introduction

This section explains the implications for the results seen in the previous sections. It explores the extent to which the assumptions made in the described model may affect the results. It then aims to explain what effect each assumption would have on the figures produced if included. There is likely not a large deviation between the results obtained in this report and that which would be produced if explicitly modelling the assumptions in this system. This means that the effects mentioned here can be used to speculate about the result, without having to directly include them in the modelling process.

The topic of this dissertation is centred around describing the dynamics and properties of the magma in each sample. The fact that the process of crystal migration is not possible under natural conditions may in fact give evidence for a much more significant result.

5.2 Crystal Settling

From much of the older literature, field observations typically regard the flow patterns seen in dykes and eroded volcanic conduits to show at least a partial result of crystal settling (Gibb & Henderson, 1992). Crystal settling is the process of crystals depositing out of suspension in the melt due to an imbalance of forces acting on the individual crystals (Gökelma, et al., 2015). For example, to induce a downwards motion, the vertical gravitational force must be larger than the sum of upwards resisting forces. This is visualised in Figure 5.1 where Gravitational Force > Buoyancy + Drag.

It is inferred from Martin & Nokes, 1988 that crystal settling is likely only relevant for cases where the Stoke's number is low. If the Stoke's number is much smaller than a value of one, in other words: $St << 1$, it can be argued that the crystals are well coupled with the melt (Dufek & Bachmann, 2010) and therefore do not settle out of the flow due to buoyancy or gravitational forces acting on the particle.



Figure 5.1*: Figure adapted from Gökelma, et al., 2015 to visualise the forces acting on a solid spherical crystal, moving vertically downwards under gravity through an incompressible melt.*

It is inferred in the Lecampion & Garagash, 2014 model that the densities of both the solid and liquid phases are equal, hence crystal settling is not a process considered in the constitutive equations there. In the natural magmatic system however, this is rarely the case. In order to test which magmas this coupling would be relevant for, equation 5.1 from Mueller, et al., 2010 is used to calculate the Stoke's number:

$$St = \frac{\rho_P a^3 \dot{\gamma}}{\lambda \mu_0} = \frac{\rho_P a^2 \dot{\gamma}}{\mu_0} \qquad \textit{Equation 5.1}$$

Where ρ_P is the particle density, a is particle radius, $\dot{\gamma}$ is the strain rate, λ is the characteristic particle length and μ_0 is the viscosity of the melt phase. Note that as $\lambda = a$ for a sphere, this equation can be simplified to that of the right-hand version.

This calculation is undertaken for all dimensional examples used in this dissertation to investigate if any of the melts are poorly coupled. It is found that for all strain rates present in

each example, the Stoke's number is always much less than one, in other words; $St << 1$. This means that, the crystals are well coupled with the melt and therefore crystal migration can be discounted as an active effect.

5.3 Implications for the Rheology of Magmas

In Section 4, it was found that crystal migration is a process that could theoretically occur on Earth given the right conditions, however the examples investigated there show that these conditions are not possible in the natural system. This includes use of the more extreme examples on Earth, which were chosen to give the best chance of seeing this process.

It is considered that the crystal volume fraction present in the Basaltic examples is too low. This, combined with the shorter conduit lengths, means that crystal migration is not present in these examples. The Silicic and Dacitic examples also do not exhibit crystal migration due to the high viscosity in both cases. This may give the impression of a negative result for the outcome of this study; however, this provides a valuable insight into the behaviour of crystal bearing magmas.

As mentioned previously, throughout the 'history' of volcanology, the non-Newtonian rheology of magmas is assumed due to the presence of crystals suspended in the liquid melt. Experiments to measure the viscosity of small-scale samples in the laboratory by studies such as Caricchi, et al., 2007 & Sonder, et al., 2006, do indeed find a non-Newtonian result. The apparent non-Newtonian behaviour seen from those studies was due to the crystals in those samples migrating. This is important to note, as this modern theory of crystal migration was not available when those earlier studies were undertaken, hence the authors of those papers did not check for crystal migration as an effect that might be occurring. This means they

missed this migration phenomenon, so could not explain the non-Newtonian result found in their samples.

However, the results from this dissertation would argue against this non-Newtonian rheology being the case for the magma on the large-scale conduit sizes investigated here. From the results of the numerical simulations, it is found that migration of the crystals during flow along the conduit does not occur for the length of conduits present in the natural system. From this, the conclusion can be drawn that the non-Newtonian results of magmas found from small-scale experiments are not up-scalable to the conduit scale size of magma flow in the crust. To put this in other words, it is found in this dissertation that crystalline magmas might in fact be homogenous and Newtonian when considered on a crustal scale.

Figure 5.2 shows a sketch of the typical flow curves exhibited from fluids with differing rheologies. The previous literature for small-scale experiments of magma rheology argue for the case of curve **b** on this diagram to show non-Newtonian 'pseudoplastic' behaviour. The results from this dissertation argue against this being the case for magma on large-scale conduit sizes. These would follow flow curve **a** as a linear relationship between the applied stress at any point and strain-rate at that point to define a Newtonian magma (Batchelor & Batchelor, 2000).

From this result, all models of magma ascent that assume a non-Newtonian rheology may need to be revisited. The list is extensive, but includes: Caricchi, et al., 2007;

Figure 5.2 removed for copyright

This figure is from Mader et al. (2013), so it isn't reproduced in this online version. Please see the original paper.

Figure 5.2: *from Mader, et al., 2013 to show the typical flow curves of* ***a*** *Newtonian,* ***b*** *pseudoplastic,* ***c*** *dilatant,* ***d*** *Bingham,* ***e*** *Hershel-Bulkley type fluids.*

Rosenberg, 2004; Rutherford, 2008; Scandone, et al., 2007; Aki & Koyanagi, 1981, etc.

One implication of this result is that strain localisation at the walls of the conduit is not as pronounced as previously thought. Following a non-Newtonian rheology, like that seen in the result of the Base example of Figure 4.1, the strain rate increases in an exponential form, resulting in very high strain rate partitioned at the walls. However, the Newtonian results of the dimensional case study examples show a Newtonian rheology where the strain rate increases in a linear form as the walls are approached, meaning this partitioning is not as pronounced as originally thought. This may have implications for the relevance of such studies as viscous heating (eg. Costa & Macedonio, 2003), viscoelastic fracturing at conduit margins (eg. Okumura, et al., 2010) and lubrication and stick-slip motion at the margins (eg. Kendrick, et al., 2012). This last point also links to the associated seismicity that has been assumed in magma movement eg. Kendrick, et al., 2014.

5.4 Effect of Bubbles

One assumption taken in this model is to neglect the presence of bubbles in the magma during ascent through the conduit. In reality, as magma ascends towards the surface, it becomes rapidly depressurised. This under pressuring of the magma causes its dissolved volatiles to exsolve, rapidly forming bubbles (Alidibirov & Dingwell, 1996).

One possible way to account for the effect of bubbles on this system is to use an effective medium approach (Sen & Mukerji, 1997). This involves assuming that where bubbles are present in the melt, they are smaller than the crystals. This allows for the liquid to be described by a new viscosity value, depending on the geometry of the bubbles. Bubble geometry has an impact on the viscosity of the liquid that is controlled by the pressure in the flow. A lower pressure will result in spherical bubbles that act as a barrier for melt movement,

and therefore increase the viscosity. On the other hand, a higher pressure would result in a lower viscosity as the liquid is able to move more rapidly around the prolate shape.

A lower viscosity of the melt would have the effect of allowing easier movements of crystals through the melt towards the centre of the flow as they are sheared away from the walls, meaning a shorter conduit length required for fully developed flow. However, a higher viscosity would have the opposite effect.

5.5 Effect of Non-Spherical Crystals

Throughout this dissertation, an approximation for the shape of crystals present in the magma is assumed to be that of incompressible spheres. In the natural system, all shapes of crystal are possible through from longer Plagioclase to flatter Pyroxene (Holness, 2015). However, due to modelling constraints and the lack of previous literature, explicit modelling of different shaped crystals is not explored here.

Crystal with a prolate shape, such as plagioclase may move through the magma melt more rapidly when the long axis is aligned in the axial direction of the flow, compared to an oblate shape crystal (Yamato, et al., 2011). This first case could have the effect of decreasing the conduit length required for fully developed flow to occur for the prolate crystals or, conversely, increasing the length when considering oblate crystals.

Field observations of crystalline dykes suggest that a common arrangement seen is that the major axis on longer crystals often lie parallel or sub-parallel to the edge of the dyke. This has been interpreted to be the result of magma flow causing the crystals to rotate and become aligned with the flow direction (Yamato, et al., 2011). This can be seen in Figure 5.3 taken from Yamato, et al., 2011 with the number of crystals in a melt-crystal suspension that are aligned with the flow direction increasing with time. Where these longer crystals occur in

the natural system, it may be the case that the length of conduit required for fully developed flow to occur is shorter than that predicted here. It is important to note that this likely wouldn't have a significant impact and the results of including these crystals are unlikely to produce a significant deviation from the results produced already.

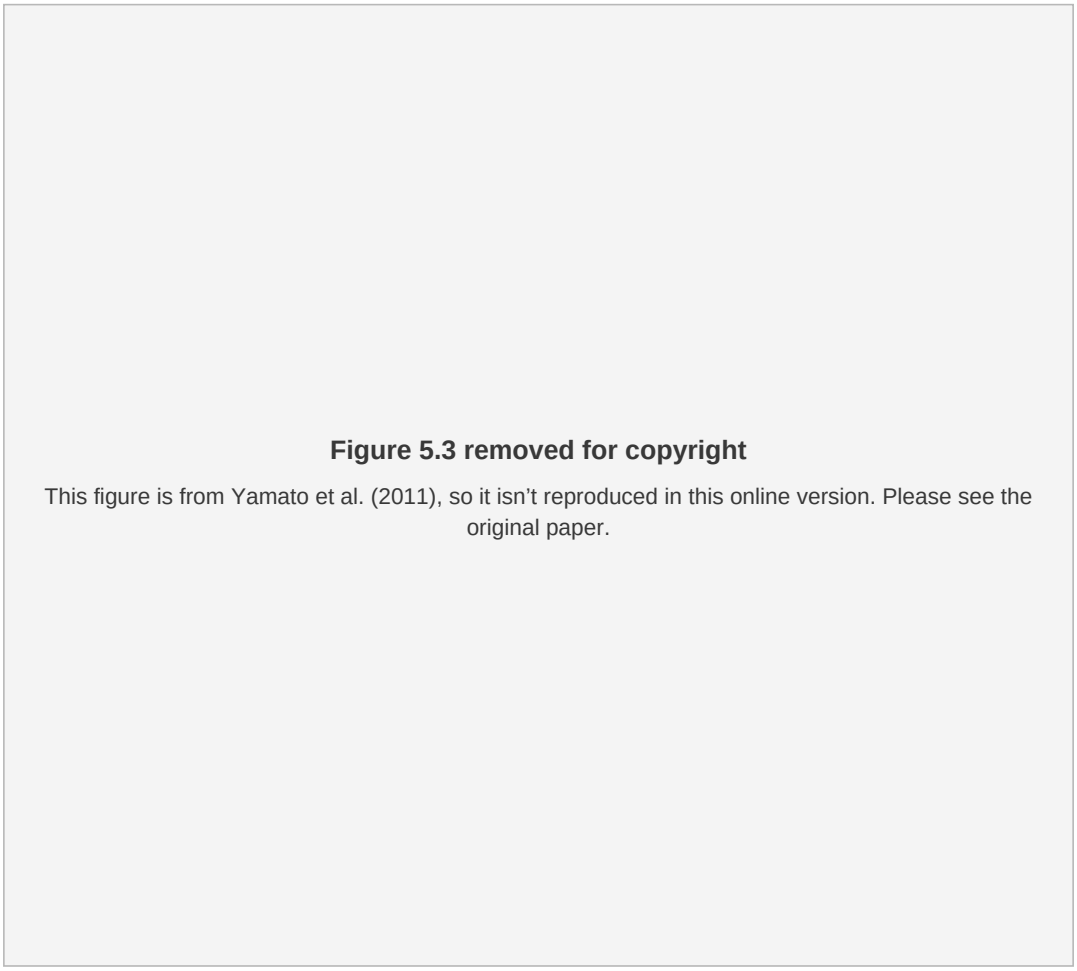


Figure 5.3*: From Yamato, et al., 2011 to visualise rectangular crystal rotation in a flowing magma. Still images of the numerical simulation taken for time,* $t = 0\ s,\ 10\ s,\ 20\ s$*. Frequency histograms of the orientation of the first*

The other effect of non-spherical crystals would be to change the value of the maximum packing crystal fraction ϕ_m that would be present in the plugged region of the flow. This is significant as this is a factor present in Equation 1 described in this dissertation. A non-spherical crystal would reduce this maximum packing fraction in the jammed region, having a direct influence on the crystal volume fraction throughout the flow.

5.6 Effect of Unsteady Conditions

The model used in this dissertation from Lecampion & Garagash, 2014 is that of a steady state model as the equations are written to be non-time dependant in Section 2. The importance of this in regard to this dissertation is that the inlet velocity at the base of the conduit is assumed to be constant in all cases. This can only be assumed to be correct if the volume of magma in the reservoir is much larger than the volume in the conduit itself (Cashman & Giordano, 2014) so the pressure in the system as a whole will not decay rapidly. If this was not the case, and the inlet velocity was not constant, this theory would no longer hold, and the equations described in Section 2 would have to be re-written with respect to time.

6 Conclusion

To conclude the results of this dissertation, the three questions set out to be answered during the Objectives and Hypotheses section will be assessed here. The hypothesis also posed of: "*The particle pressure acting on the crystals in magmas can be relevant under natural conditions*" is proven to be false. The results from this dissertation have shown that there is no known situation on Earth where crystal migration can occur under natural conditions.

6.1 Question 1: To what extent does crystal migration occur within a natural magmatic setting?

Crystal migration is most effective with a low viscosity melt, high crystal volume fraction and large particle sizes. The geometry of the volcanic conduit itself also plays a pivotal role in determining if fully developed flow is achieved before the magma reaches the surface. This could mean that if a highly crystalline basaltic magma, resulting in low viscosity was situated in a relatively long conduit length with a small radius, then fully developed flow

may indeed be possible under these conditions. This was seen in the 'Base' example of Figure 4.1, used as the conditions that were mostly likely to exhibit the effects of crystal migration. This however does not act as a real case study for the natural system. In the real case study examples, even under the 'extreme' examples, chosen as the studies most likely to display these effects, were investigated it is found that there is no situation on Earth where fully developed flow may be realised. Hence, in answer to the first question posed at the start of this dissertation, crystal migration as a process that occurs in the volcanic conduit should not be considered possible in this system. This does not mean crystal migration is not possible, but that the volcanic conduits found on Earth are not long enough to show these effects.

6.2 Question 2: What are the effects on the results when the assumptions used in the calculations are challenged?

The assumptions made that would most likely have the biggest effect on the results if challenged are explored in the Discussion section of this dissertation. These effects are not explicitly modelled, but speculation on the outcome is considered there in order to assess the relative uncertainty in each case. There are other assumptions used during the calculations, however it is likely these would not have a significant impact on the outcome, so are not discussed here.

The main assumptions are that of including bubbles in the liquid melt alongside the crystals, and it is also considered that the magma pressure in the system would play a role in changing the viscosity of the melt by affecting bubble geometry. An effective medium approach could be adopted here to use a new value for the viscosity of the melt depending on the bubble shapes.

Another factor that may play an important role is the effect on non-spherical crystals. When the long axis of a prolate-shaped crystal is aligned with the flow direction, it may travel faster through the melt, decreasing the length conduit length required for fully developed flow to evolve. The other effect of non-spherical crystals would be to change the value of the maximum packing fraction ϕ_m used in equation 1 of the dissertation, hence changing the concentration of crystals dispersed throughout the flow.

6.3 Question 3: What does this mean for the rheology of the magma if crystal migration is or is not occurring?

The seemingly negative result that crystal migration does not occur in any volcanic conduits on Earth in the natural system can be used to deduce properties about the magma rheology under these conditions.

It is widely assumed throughout volcanology that the presence of crystals in the melt leads to the non-Newtonian behaviour seen in previous studies (eg. Caricchi, et al., 2007; Sonder, et al., 2006). Typically, these previous studies are carried out at significantly smaller scales than that described in this dissertation. The viscosities of these small samples are then measured and a non-Newtonian rheology is deduced.

As the results in all of the dimensional real case study examples do not exhibit the effects of crystal migration, it can be concluded that the crystals in these large-scale magma flows are not migrating. This is contrary to the results of experiments in previous studies. Hence, the non-Newtonian rheology found from those studies is an experimental artefact and is not up-scalable to the conduit sizes investigated here.

This may have significant implications for many numerical models of magma ascent as they are based on the presumption that the magma is non-Newtonian. This means that, potentially, there may be significant fallacies between the results found in those previous studies and the true model. Several of the physical phenomena projected to be occurring from the results of such studies may also need to be revisited following this new information.

7. References

Aki, K. & Koyanagi, R., 1981. Deep volcanic tremor and magma ascent mechanism under Kilauea, Hawaii. *Journal of Geophysical Research: Solid Earth,* 86(B8), pp. 7095-7109.

Alidibirov, M. & Dingwell, D. B., 1996. Magma fragmentation by rapid decompression. *Nature,* 380(1), pp. 146-148.

Bachmann, O. & Dungan, M. A., 2002. Temperature-induced Al-zoning in hornblendes of the Fish Canyon magma, Colorado. *American Mineralogist,* 87(8-9), pp. 1062-1076.

Bardintzeff, J.-M., Miskivsky, J.-C., Traineau, H. & Westercamp, D., 1989. The recent pumice eruptions of Mt. Pelée volcano, Martinique. Part II: Grain-size studies and modeling of the last Plinian phase P1. *Journal of Volcanology and Geothermal Research,* 38(1-2), pp. 35-48.

Barrière, M., 1976. Flowage Differentiation: Limitation of the "Bagnold Effect" to the Narrow Intrusions. *Contributions to Mineralogy and Petrology,* 55(1), pp. 139-145.

Batchelor, C. K. & Batchelor, G. K., 2000. *An Introduction to Fluid Dynamics.* 1st ed. Cambridge: Cambridge University Press.

Blake, S. & Campbell, I. H., 1986. The dynamics of magma-mixing during flow in volcanic conduits. *Contributions to Mineralogy and Petrology,* 94(1), pp. 72-81.

Boyer, F., Guazzelli, É. & Pouliquen, O., 2011. Unifying Suspension and Granular Rheology. *Physical Review Letters,* 107(18), pp. 188301-188306.

Brey, G. P. & Köhler, 1990. Geothermobarometry in Four-phase Lherzolites II. New Thermobarometers, and Practical Assessment of Existing Thermobarometers. *Journal of Petrology,* 31(6), pp. 1353-1378.

Bruce, P. M. & Huppert, H. E., 1990. Solidification and melting along dykes by the laminar flow of basaltic magma. *Magma transport and Storage,* 1(1), pp. 87-101.

Caricchi, L. et al., 2007. Non-Newtonian rheology of crystal-bearing magmas and implications for magma ascent dynamics. *Earth and Planetary Science Letters,* 264(3-4), pp. 402-419.

Cashman, K. V. & Giordano, G., 2014. Calderas and magma reservoirs. *Journal of Volcanology and Geothermal Research,* 288(1), pp. 28-45.

Cassidy, M. et al., 2019. Explosive Eruptions With Little Warning: Experimental Petrology and Volcano Monitoring Observations From the 2014 Eruption of Kelud, Indonesia. *Geochemistry, Geophysics, Geosystems,* 20(8), pp. 4218-4247.

Correy, C. E., 1988. *Laccoliths: mechanics of emplacement and growth.* 220 ed. Boulder: Geological Society of America, Inc..

Costa, A. & Macedonio, G., 2003. Viscous heating in fluids with temperature-dependent viscosity: implications for magma flows. *Nonlinear Processes in Geophysics,* 10(6), pp. 545-555.

Dufek, J. & Bachmann, O., 2010. Quantum magmatism: Magmatic compositional gaps generated by melt-crystal dynamics. *Geology,* 38(1), pp. 687-690.

Frigaard, I. A. & Ryan, D. P., 2004. Flow of a visco-plastic fluid in a channel of slowly varying width. *Journal of Non-Newtonian Fluid Mechanics,* 123(1), pp. 67-83.

Gibb, F. G. F. & Henderson, M. B., 1992. Convection and crystal settling in sills. *Contributions to Mineralogy and Petrology,* 109(1), pp. 538-545.

Gilbert, J. S. & Lane, S. J., 2008. The consequences of fluid motion in volcanic conduits. *Fluid Motions in Volcanic Conduits ,* 307(1), pp. 1-10.

Giordano, D., Russell, J. K. & Dingwell, D. B., 2008. Viscosity of magmatic liquids: A model. *Earth and Planetary Science Letters,* 271(1-4), pp. 123-134.

Gökelma, M. et al., 2015. Observation on inclusion settling by LiMCA and PoDFA Analysis in Aluminium Melts. *Internation Aluminium Journal,* 91(1), pp. 56-61.

Goto, A., 1999. A new model for volcanic earthquake at Unzen Volcano: Melt Rupture Model. *Geophysical Research Letters,* 26(16), pp. 2541-2544.

Goto, Y., Miyoshi, M., Danhara, T. & Tomiya, A., 2020. Evolution of the Quaternary silicic volcanic complex of Shiribetsu, Hokkaido, Japan: an example of ignimbrite shield volcanoes in an island arc setting. *International Journal of Earth Sciences,* 109(1), pp. 2619-2642.

Green, D. H. & Ringwood, A. E., 1967. The genesis of basaltic magmas. *Contributions to Mineralogy and Petrology,* 15(1), pp. 103-190.

Guazzelli, E. & Pouliquen, O., 2018. Rheology of Dense Granular Suspensions. *Journal of Fluid Mechanics,* 852(1), pp. 1-73.

Heap, M. J. et al., 2014. Microstructural controls on the physical and mechanical properties of edifice-forming andesites at Volcán de Colima, Mexico. *Journal of Geophysical Research: Solid Earth,* 119(4), pp. 2925-2963.

Hoblitt, R. P. & Harmon, R. S., 1993. Bimodal Density Distribution of Cryptodome Dacite from the 1980 Eruption of Mount St. Helens, Washington. *Bulletin of Volcanology,* 55(1), pp. 421-437.

Holness, M. B., 2015. Plagioclase Growth Rates Control Three-grain Junction Geometry in Dolerites and Gabbros. *Journal of Petrology,* 56(11), pp. 2117-2144.

Ishibashi, H., 2009. Non-Newtonian behavior of plagioclase-bearing basaltic magma: Subliquidus viscosity measurement of the 1707 basalt of Fuji volcano, Japan. *Journal of Volcanology and Geothermal Research,* 181(1-2), pp. 78-88.

Kendrick, J. E. et al., 2012. Extreme frictional processes in the volcanic conduit of Mount St. Helens (USA) during the 2004–2008 eruption. *Journal of Structural Geology,* 38(1), pp. 61-76.

Kendrick, J. E. et al., 2014. Volcanic drumbeat seismicity caused by stick-slip motion and magmatic frictional melting. *Nature Geoscience,* 7(1), pp. 438-442.

Komar, P. D., 1972. Flow Differentiation in Igneous Dikes and Sills: Profiles of Velocity and Phenocryst Concentration. *GSA Bulletin,* 83(11), pp. 3443-3448.

La Spina, G. et al., 2021. Explosivity of basaltic lava fountains is controlled by magma rheology, ascent rate and outgassing. *Earth and Planetary Science Letters,* 553(0012), p. 116658.

Lavallée, Y., Hess, K. -U., Cordonnier, B. & Dingwell, D. B., 2007. Non-Newtonian rheological law for highly crystalline dome lavas. *Geology,* 35(9), pp. 843-846.

Lavallée, Y. et al., 2012. Magmatic architecture of dome-building eruptions at Volcán de Colima, Mexico. *Bulletin of Volcanology,* 74(1), pp. 249-260.

Lecampion, B. & Garagash, D. I., 2014. Combined flow of suspensions modelled by a frictional rheology. *Journal of Fluid Mechanics,* 759(1469), pp. 197-235.

Luhr, J. F., 2002. Petrology and geochemistry of the 1991 and 1998–1999 lava flows from Volcán de Colima, México: implications for the end of the current eruptive cycle. *Journal of Volcanology and Geothermal Research,* 117(1-2), pp. 169-194.

Mader, H. M., Llewellin, E. W. & Mueller, S. P., 2013. The rheology of two-phase magmas: A review and analysis. *Journal of Volcanology and Geothermal Research,* 257(1), pp. 135-158.

Martel, C. et al., 1998. Magma storage conditions and control of eruption regime in silicic volcanoes: experimental evidence from Mt. Pelée. *Earth and Planetary Science Letters,* 156(1-2), pp. 89-99.

Martel, C. & Poussineau, S., 2007. Diversity of eruptive styles inferred from the microlites of Mt Pelée andesite (Martinique, Lesser Antilles). *Journal of Volcanology and Geothermal Research,* 166(3-4), pp. 233-254.

Martin, D. & Nokes, R., 1988. Crystal settling in a vigorously convecting magma chamber. *Nature,* 332(1), pp. 534-536.

McCanta, M. C., Rutherford, M. J. & Hammer, J. E., 2007. Pre-eruptive and syn-eruptive conditions in the Black Butte, California dacite: Insight into crystallization kinetics in a silicic magma system. *Journal of Volcanology and Geothermal Research,* 160(3-4), pp. 263-284.

Middlemost, E. A. K., 1994. Naming materials in the magma/igneous rock system. *Earth-Science Reviews,* 37(3-4), pp. 215-224.

Mueller, S., Llewellin, E. W. & Mader, H. M., 2010. The rheology of suspensions of solid particles. *Proceedings of The Royal Society: A,* 466(1), pp. 1201-1228.

Nakada, M., Motomura, Y., Shimizu & Hiroshi, 1995. Manner of magma ascent at Unzen Volcano (Japan). *Geophysical Research Letters,* 22(5), pp. 567-570.

Nakada, S. & Motomura, Y., 1999. Petrology of the 1991–1995 eruption at Unzen: effusion pulsation and groundmass crystallization. *Journal of Volcanology and Geothermal Research,* 89(1-4), pp. 173-196.

Noguchi, S., Toramaru, A. & Nakada, S., 2008. Relation between microlite textures and discharge rate during the 1991–1995 eruptions at Unzen, Japan. *Journal of Volcanology and Geothermal Research,* 175(1-2), pp. 141-155.

Nott, P. R. & Brady, J. F., 1994. Pressure-driven flow of suspensions: simulation and theory. *Journal of Fluid Mechanics,* 275(1), pp. 157-199.

Okumura, S. et al., 2010. Shear deformation experiments on vesicular rhyolite: Implications for brittle fracturing, degassing, and compaction of magmas in volcanic conduits. *Journal of Geophysical Research: Solid Earth,* 115(B6), p. B06201.

Petford, N., Lister, J. R. & Kerr, R. C., 1994. The ascent of felsic magmas in dykes. *Lithos,* 32(1-2), pp. 161-168.

Rodgers, S. E., Kwak, D. & Kiris, C., 1991. Steady and unsteady solutions of the incompressible Navier-Stokes equations. *AIAA Journal,* 29(4), pp. 603-610.

Rosenberg, C. L., 2004. Shear zones and magma ascent: A model based on a review of the Tertiary magmatism in the Alps. *Tectonics,* 23(3), p. TC3002.

Rutherford, M. J., 2008. Magma Ascent Rates. *Reviews in Mineralogy and Geochemistry,* 69(1), pp. 241-271.

Ryerson, F. J., Weed, H. C. & Piwinskii, A. J., 1988. Rheology of subliquidus magmas: 1. Picritic compositions. *Journal of Geophysical Research: Solid Earth,* 93(B4), pp. 3421-3436.

Sakamaki, T., 2017. Density of Hydrous Magma. *Chemical Geology ,* 475(1), pp. 135-139.

Scandone, R., Cashman, K. V. & Malone, S. D., 2007. Magma supply, magma ascent and the style of volcanic eruptions. *Earth and Planetary Science Letters,* 253(3-4), pp. 513-529.

Sen, S. & Mukerji, T., 1997. Diffusion and viscosity in silicate liquids: Percolation and effective medium theories. *Geophysical Research Letters,* 24(9), pp. 1015-1018.

Slezin, Y. B., 2003. The mechanism of volcanic eruptions (a steady state approach). *Journal of Volcanology and Geothermal Research,* 122(1-2), pp. 7-50.

Sonder, I., Zimanowski, B. & Büttner, R., 2006. Non-Newtonian viscosity of basaltic magma. *Geophysical Research Letters,* 33(2), p. L02303.

Sparks, R. S. J., 2003. Dynamics of magma degassing. *Geological Society Publications,* 213(1), pp. 5-22.

Sparks, R. S. J., Meyer, P. & Sigurdsson, H., 1980. Density variation amongst mid-ocean ridge basalts: Implications for magma mixing and the scarcity of primitive lavas. *Earth and Planetary Science Letters,* 46(3), pp. 419-430.

Spiegelhalter, D. J., Best, N. G., Carlin, B. P. & Linde, A. V. D., 2002. Bayesian measures of model complexity and fit. *Journal of the Royal Statistical Society: Series B (Statistical Methodology),* 64(4), pp. 583-639.

Stickel, J. J. & Powell, R. L., 2005. Fluid Mechanics and Rheology of Dense Suspensions. *Annual Review of Fluid Mechanics,* 37(1), pp. 129-149.

Winkler, H. G. F., 1949. Crystallization of basaltic magma as recorded by variation of crystal-size in dikes. *Mineralogical magazine and journal of the Mineralogical Society ,* 28(205), pp. 557-574.

Yamato, P., Tartèse, Duretz, T. & May, D. A., 2011. Numerical modelling of magma transport in dykes. *Tectonophysics,* 526-529(1), pp. 97-109.

8. Appendix

Quantity	Symbol	Unit
Friction Coefficient	μ	-
Initial Friction Coefficient	μ_0	-
Friction Coefficient at Jamming Limit	μ_1	-
Particle/Crystal Volume Fraction	ϕ	-
Jamming Value of Particle/ Crystal Volume Fraction	ϕ_m	-
Initial Particle/Crystal Volume Fraction	ϕ_0	-
Gap Averaged Particle/ Crystal Volume Fraction	$\langle\phi\rangle$	-
Particle/Crystal Volume Fraction at Wall	ϕ_w	-
Dimensionless Viscous Number	I	-
Initial Dimensionless Viscous Number	I_0	-
Compressibility Coefficient	β	-
Inertial Number	I_n	-
Inertial Time of Particle/ Crystal Rearrangement	t_{micro}	s
Time of Strain	t_{macro}	s
Diameter of Particle/Crystal (Sphere)	d	m
Density of Particle/Crystal	ρ_p	kg m^{-3}
Confining Pressure of System	P^p	Pa
Strain	γ	-
Strain Rate	$\dot{\gamma}$	s^{-1}
Strain Rate in the Axial Direction	$\dot{\gamma}_z$	s^{-1}
Viscosity of interstitial fluid/ melt	η_f	Pa s

Shear Stress	τ	Pa
Particle Normal Stress	σ_n'	Pa
Phase Velocity in Axial Direction	v_z	m s^{-1}
Gap Averaged Axial Velocity	$\langle v_z \rangle$	m s^{-1}
Phase Velocity in Radial Direction	v_r	m s^{-1}
Pressure Gradient	∇P	Pa m^{-1}
Mean Pressure Gradient	$\lvert \nabla p \rvert$	Pa m^{-1}
Initial Mean Pressure Gradient	$\lvert \nabla p_0 \rvert$	Pa m^{-1}
Number of Nodes in Axial Direction	N_x	-
Step Size in Axial Direction	dx	-
Number of Nodes in Radial Direction	N_r	-
Position Along Axial Direction	z	m
Position Along Radial Direction	r	m
Time	t	s
Inelastic Storage Coefficient	S	-
Scaled Permeability	κ	-
Hinderance Function	f	-
Experimentally Determined Exponent	α	-
Development Length Scale	L	-
Radius of Pipe/Conduit	H	m
Radius of Particles/Crystals	a	m
Aspect Ratio	δ	-
Stoke's Number	St	-
Characteristic Particle Length	λ	m

Table 7.1: List of all Quantities used in calculation undertaken in this dissertation and their respective symbols and units.

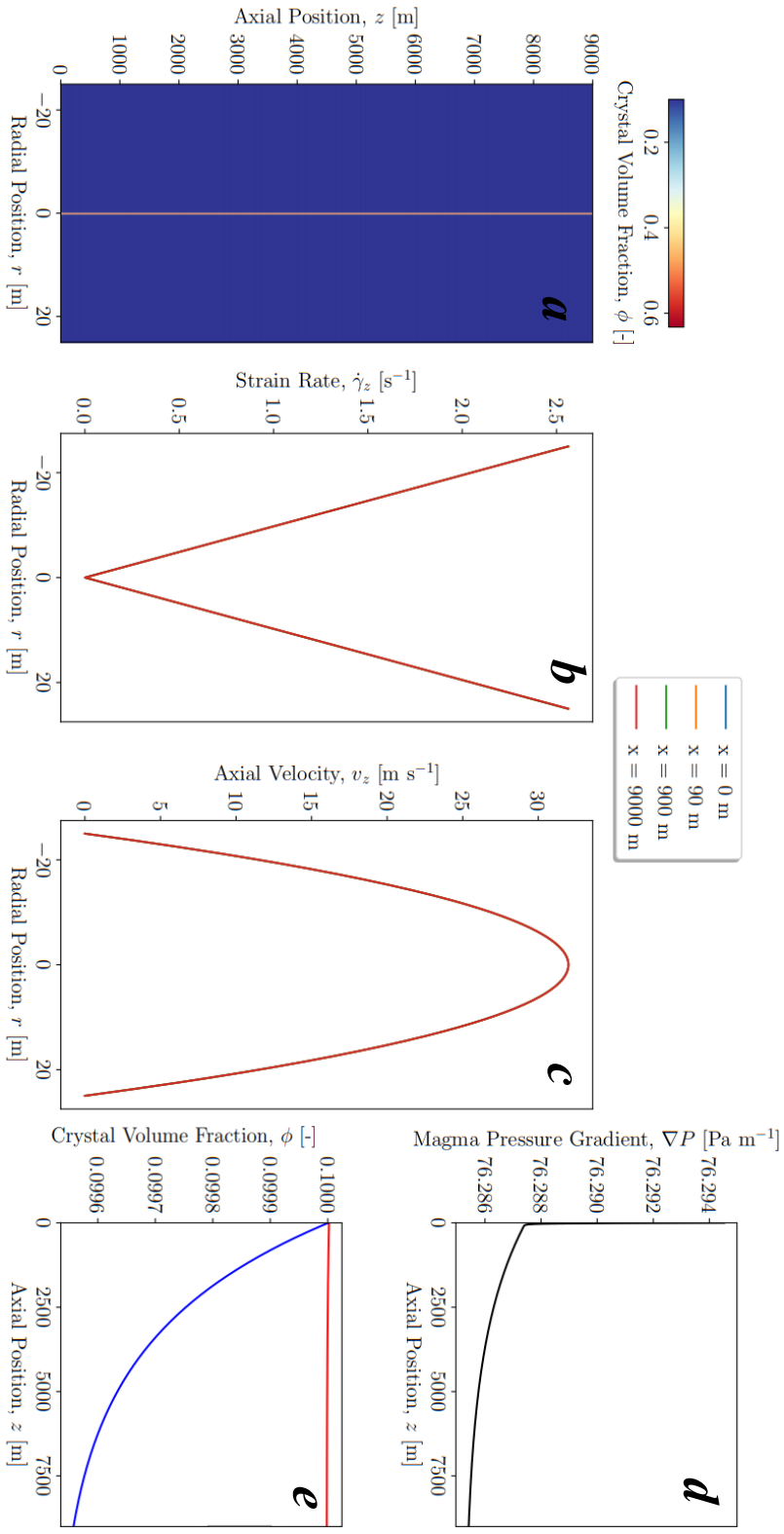


Figure 7.1*: All plots created from the code used in this dissertation for the Basaltic Example of Mt. Etna. Input parameters to create these figures correspond to Table 7.2 in this Appendix.* ***a*** *is the crystal volume fraction plot for the conduit space,* ***b*** *is the axial strain rate along the conduit,* ***c*** *is the axial velocity along the conduit,* ***d*** *is the magma pressure gradient along the conduit and* ***e*** *is the gap averaged phi value for both the centre and wall of the flow.*

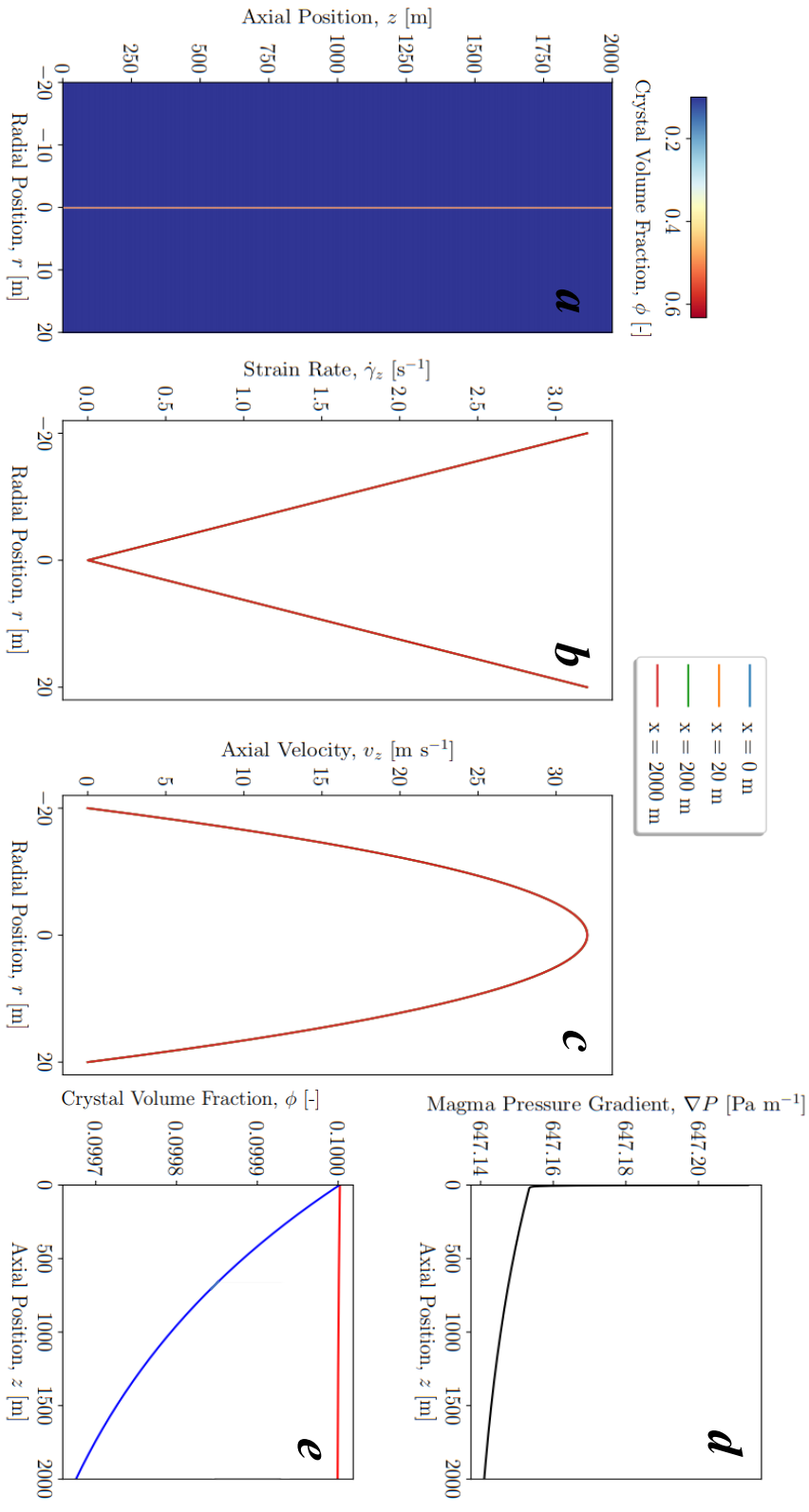


***Figure 7.2**: All plots created from the code used in this dissertation for the Basaltic Example of Kilauea. Input parameters to create these figures correspond to Table 7.3 in this Appendix. **a** is the crystal volume fraction plot for the conduit space, **b** is the axial strain rate along the conduit, **c** is the axial velocity along the conduit, **d** is the magma pressure gradient along the conduit and **e** is the gap averaged phi value for both the centre and wall of the flow.*

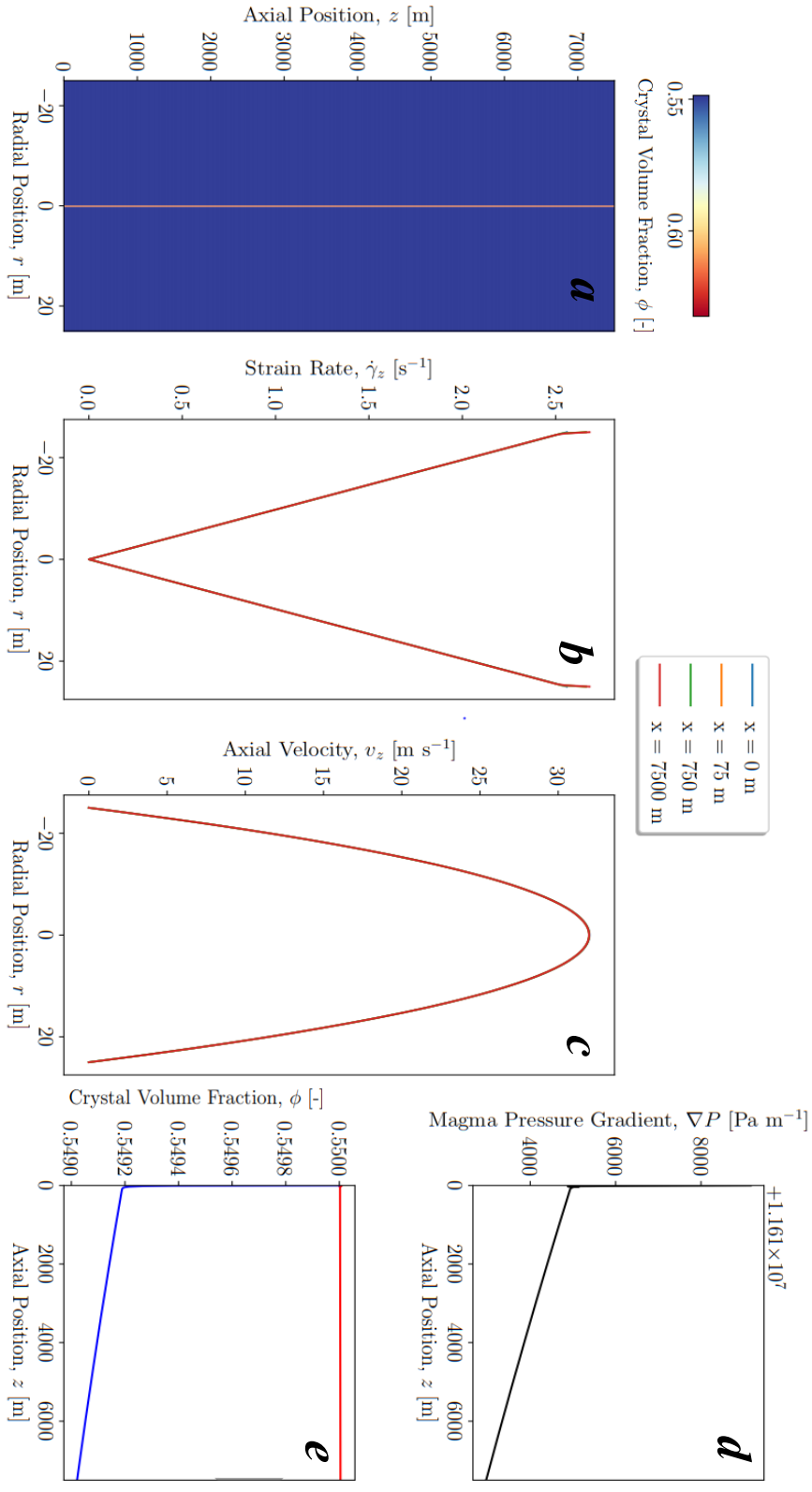


***Figure 7.3**: All plots created from the code used in this dissertation for the Dacitic Example of Unzen. Input parameters to create these figures correspond to Table 7.4 in this Appendix. **a** is the crystal volume fraction plot for the conduit space, **b** is the axial strain rate along the conduit, **c** is the axial velocity along the conduit, **d** is the magma pressure gradient along the conduit and **e** is the gap averaged phi value for both the centre and wall of the flow.*

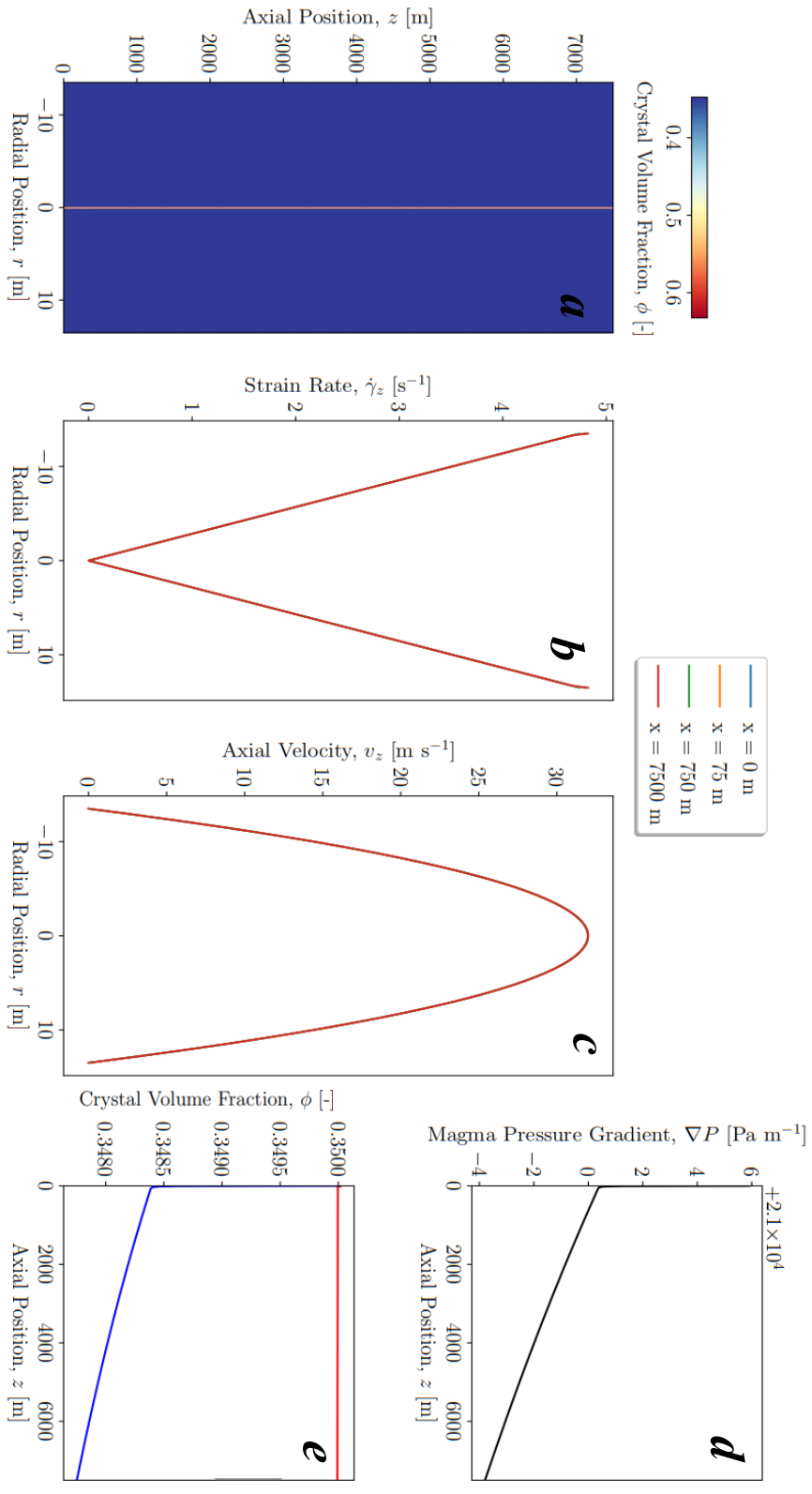


***Figure 7.4**: All plots created from the code used in this dissertation for the Andesitic Example of Volcan de Colima. Input parameters to create these figures correspond to Table 7.5 in this Appendix. **a** is the crystal volume fraction plot for the conduit space, **b** is the axial strain rate along the conduit, **c** is the axial velocity along the conduit, **d** is the magma pressure gradient along the conduit and **e** is the gap averaged phi value for both the centre and wall of the flow.*

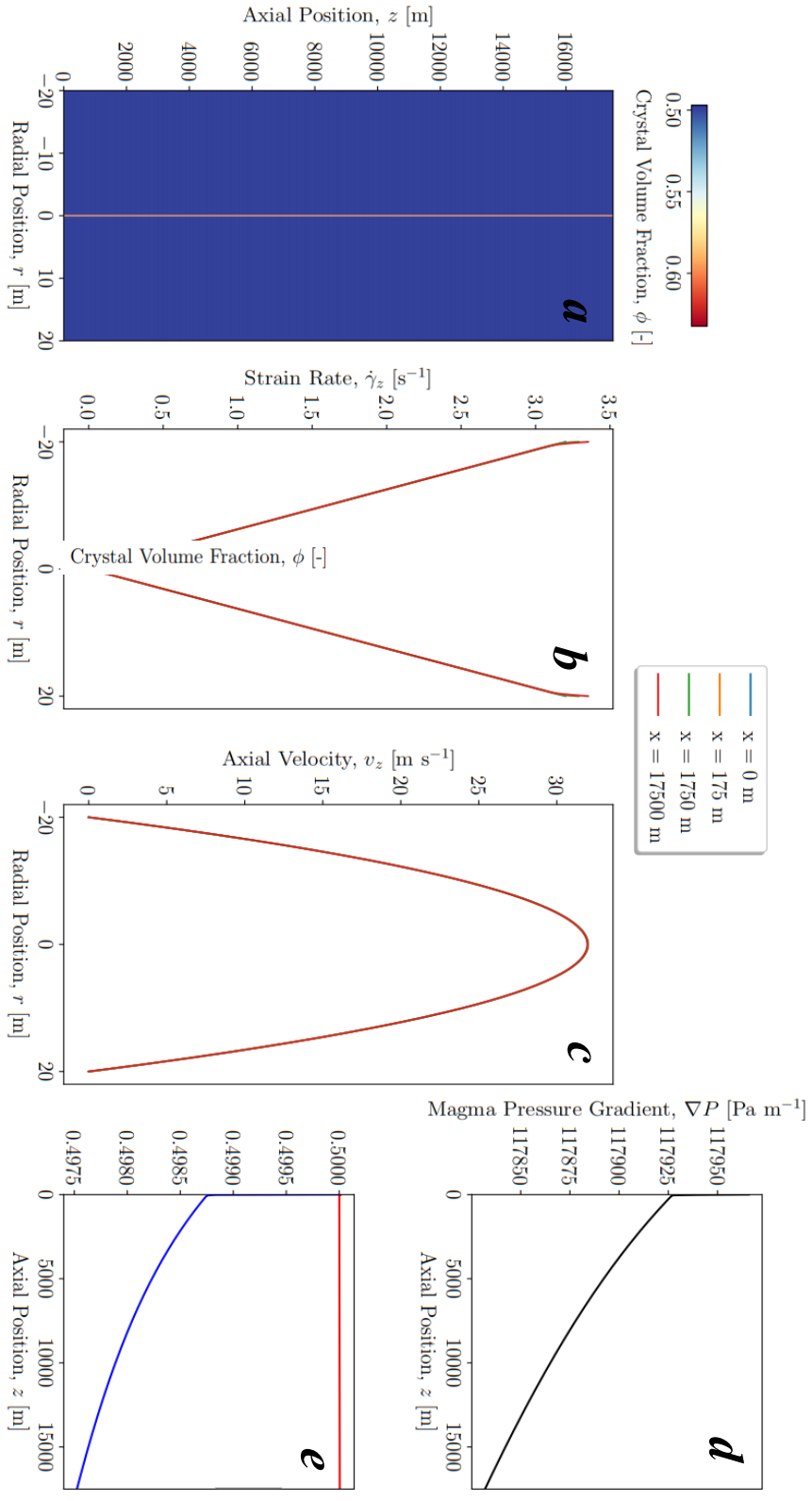


***Figure 7.5**: All plots created from the code used in this dissertation for the Andesitic Example of Fish Canyon. Input parameters to create these figures correspond to Table 7.6 in this Appendix. **a** is the crystal volume fraction plot for the conduit space, **b** is the axial strain rate along the conduit, **c** is the axial velocity along the conduit, **d** is the magma pressure gradient along the conduit and **e** is the gap averaged phi value for both the centre and wall of the flow.*

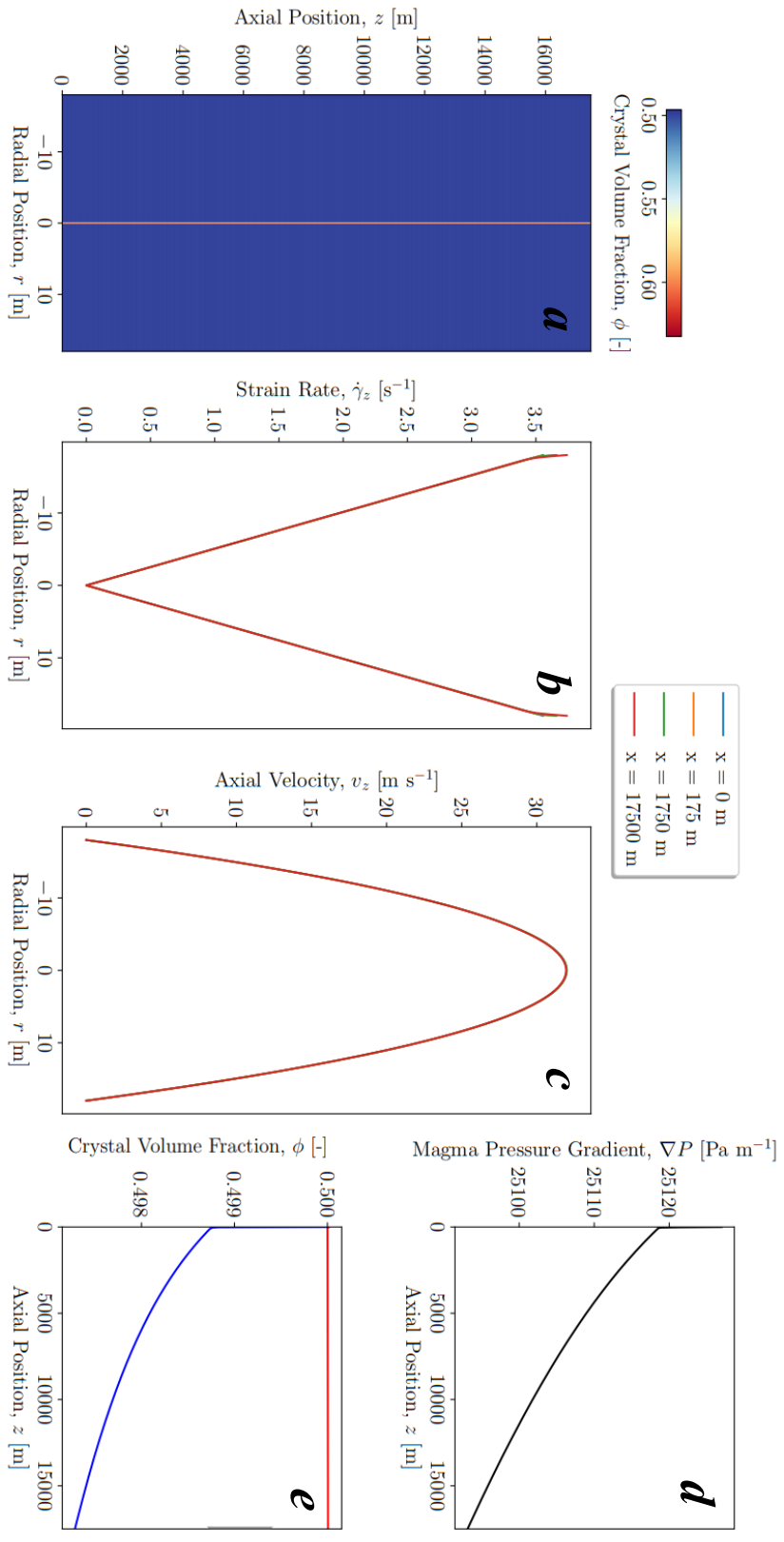


***Figure 7.6**: All plots created from the code used in this dissertation for the Basaltic Example of Pelee. Input parameters to create these figures correspond to Table 7.7 in this Appendix. **a** is the crystal volume fraction plot for the conduit space, **b** is the axial strain rate along the conduit, **c** is the axial velocity along the conduit, **d** is the magma pressure gradient along the conduit and **e** is the gap averaged phi value for both the centre and wall of the flow.*

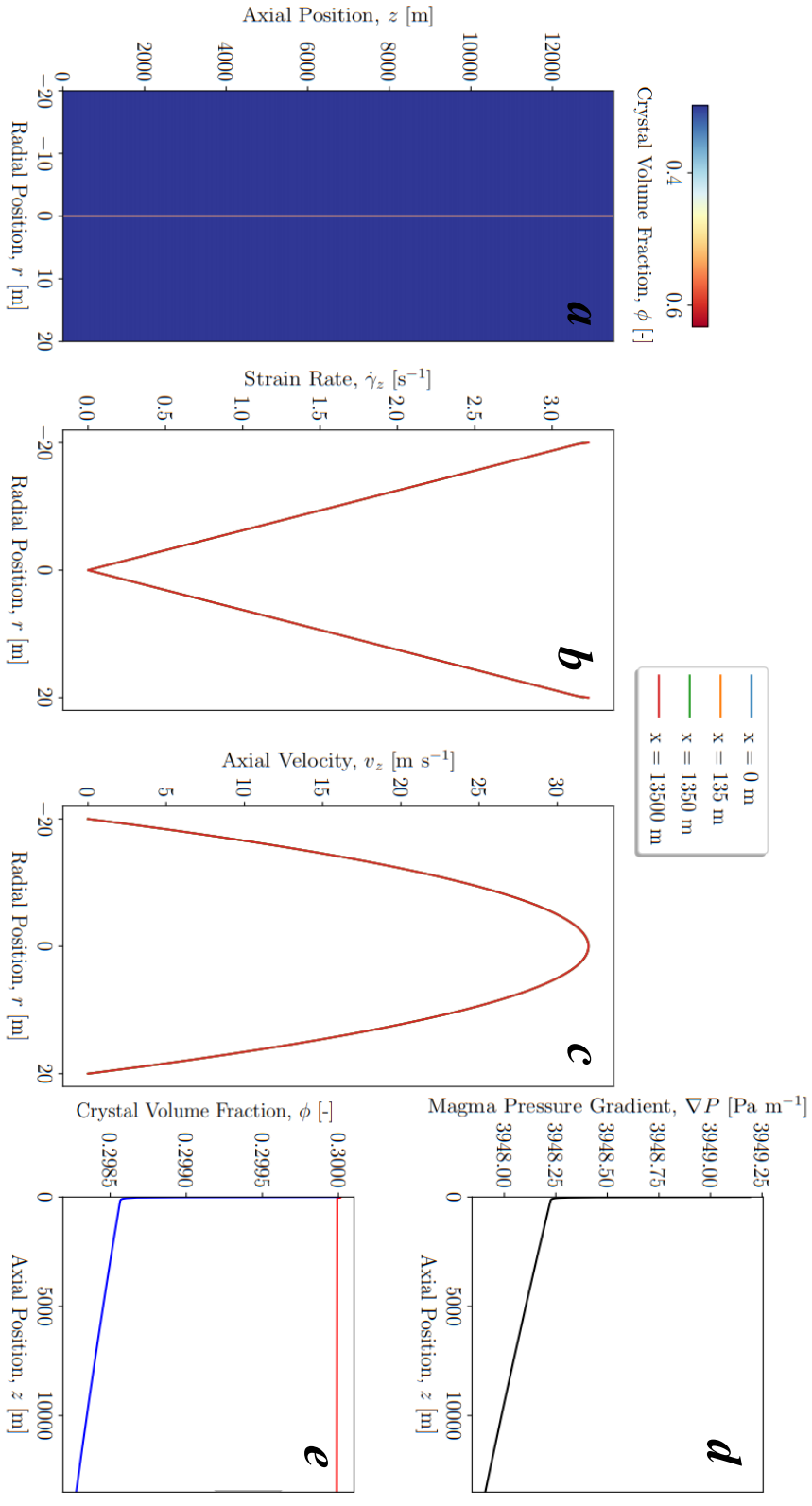


***Figure 7.7**: All plots created from the code used in this dissertation for the Dacitic Example of Black Butte. Input parameters to create these figures correspond to Table 7.8 in this Appendix. **a** is the crystal volume fraction plot for the conduit space, **b** is the axial strain rate along the conduit, **c** is the axial velocity along the conduit, **d** is the magma pressure gradient along the conduit and **e** is the gap averaged phi value for both the centre and wall of the flow.*

Example	Property	Value	Unit	Reference
Kilauea	Conduit Length	3000	m	La Spina, et al., 2021
	Crystal Content	0.1	-	La Spina, et al., 2021
	Water Concentration	0.7	wt %	La Spina, et al., 2021
	Glass Composition	-	-	La Spina, et al., 2021
	Viscosity	84.19	Pa s	Using Giordano, et al., 2008
	Conduit Radius	20	m	La Spina, et al., 2021
	Temperature	1150	°C	La Spina, et al., 2021
Unzen	Conduit Length	7500	m	Cassidy, et al., 2019
	Crystal Content	0.55	-	Lavallee, et al., 2007
	Water Concentration	0.18	wt %	Nakada & Motomura, 1999
	Glass Composition	-	-	Nakada, et al., 1995
	Viscosity	439862.78	Pa s	Using Giordano, et al., 2008
	Conduit Radius	25	m	Goto, 1999
	Eruption Temperature	1000	°C	Cassidy, et al., 2019
	Crystal Size	3.00E-04	m	Noguchi, et al., 2008
	Crystal Density	2200	kg m^{-3}	Hoblitt & Harmon, 1993

Table 7.4: *Input parameters used in the code to generate the figures seen in figure 7.3 for the example of Unzen. The property, value, unit and respective reference is included to give a comprehensive understanding of the origin of the figures produced.*

Example	Property	Value	Unit	Reference
Volcán de Colima	Conduit Length	7500	m	Cassidy, et al., 2019
	Crystal Content	0.55	-	Luhr, et al., 2002
	Water Concentration	3.4	wt %	Luhr, 2002
	Glass Composition	-	-	Lavallee, et al., 2012
	Viscosity	12.18	Pa s	Using Giordano, et al., 2008
	Conduit Radius	13.5	m	Luhr, 2002
	Temperature	1150	^{o}C	Cassidy, et al., 2019
	Crystal Size	1.00E-03	m	Heap, et al., 2014
	Crystal Density	2700	$kg\ m^{-3}$	Sparks, et al., 1980

Table 7.5: *Input parameters used in the code to generate the figures seen in figure 7.4 for the example of Volcan de Colima. The property, value, unit and respective reference is included to give a comprehensive understanding of the origin of the figures produced.*

Example	Property	Value	Unit	Reference
Fish Canyon	Conduit Length	17500	m	Cassidy, et al., 2019
	Crystal Content	0.5	-	Cassidy, et al., 2019
	Water Concentration	3.9	wt %	Bachmann, et al., 2002
	Glass Composition	-	-	Bachmann, et al., 2002
	Viscosity	12518.98	Pa s	Using Giordano, et al., 2008
	Conduit Radius	20	m	Bachmann, et al., 2002
	Temperature	850	^{o}C	Cassidy, et al., 2019
	Crystal Size	1.00E-03	m	Bachmann, et al., 2002
	Crystal Density	2450	$kg\ m^{-3}$	Sakamaki, 2017

Table 7.6: *Input parameters used in the code to generate the figures seen in figure 7.5 for the example of Fish Canyon. The property, value, unit and respective reference is included to give a comprehensive understanding of the origin of the figures produced.*

Example	Property	Value	Unit	Reference
Pelee	Conduit Length	17500	m	Cassidy, et al., 2019
	Crystal Content	0.5	-	Martel & Poussineau, 2007
	Water Concentration	5.2	wt %	Martel, et al., 1998
	Glass Composition	-	-	Martel, et al., 1998
	Viscosity	2159.92	Pa s	Using Giordano, et al., 2008
	Conduit Radius	18	m	Bardintzeff, et al., 1989
	Temperature	1000	^{o}C	Cassidy, et al., 2019
	Crystal Size	1.00E-03	m	Martel & Poussineau, 2007
	Crystal Density	2700	kg m^{-3}	Sparks, et al., 1980

Table 7.7: *Input parameters used in the code to generate the figures seen in figure 7.6 for the example of Pelee. The property, value, unit and respective reference is included to give a comprehensive understanding of the origin of the figures produced.*

Example	Property	Value	Unit	Reference
Black Butte	Conduit Length	13500	m	Cassidy, et al., 2019
	Crystal Content	0.3	-	Cassidy, et al., 2019
	Water Concentration	4.5	wt %	McCanta, et al., 2007
	Glass Composition	-	-	McCanta, et al., 2007
	Viscosity	3594.38	Pa s	Using Giordano, et al., 2008
	Conduit Radius	20	m	McCanta, et al., 2007
	Temperature	900	^{o}C	Cassidy, et al., 2019
	Crystal Size	1.00E-03	m	McCanta, et al., 2007
	Crystal Density	2200	kg m^{-3}	Hoblitt & Harmon, 1993

Table 7.8: *Input parameters used in the code to generate the figures seen in figure 7.7 for the example of Black Butte. The property, value, unit and respective reference is included to give a comprehensive understanding of the origin of the figures produced.*